Journal Pre-proof

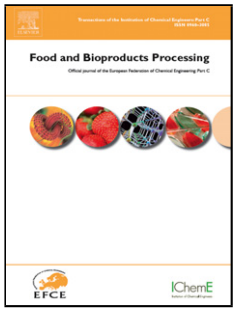

Scale-up and optimization of the spray drying conditions for the development of functional microparticles based on chia oil

María Gabriela Bordón, Noelia Pía Ximena Alasino, Álvaro Villanueva-Lazo, Cecilio Carrera-Sánchez, Justo Pedroche-Jiménez, María del Carmen Millán-Linares, Pablo Daniel Ribotta, Marcela Lilian Martínez

PII: S0960-3085(21)00125-5

DOI: https://doi.org/10.1016/j.fbp.2021.08.006

Reference: FBP 1484

To appear in: *Food and Bioproducts Processing*

Received Date: 15 June 2021

Revised Date: 5 August 2021

Accepted Date: 22 August 2021

Please cite this article as: Bordón MG, Alasino NPX, Villanueva-Lazo Á, Carrera-Sánchez C, Pedroche-Jiménez J, Millán-Linares MdC, Ribotta PD, Martínez ML, Scale-up and optimization of the spray drying conditions for the development of functional microparticles based on chia oil, *Food and Bioproducts Processing* (2021), doi: https://doi.org/10.1016/j.fbp.2021.08.006

Scale-up and optimization of the spray drying conditions for the development of functional microparticles based on chia oil

María Gabriela Bordón[1,2]; Noelia Pía Ximena Alasino[3,5]; Álvaro Villanueva-Lazo[6]; Cecilio Carrera-Sánchez[8]; Justo Pedroche-Jiménez[6]; María del Carmen Millán-Linares[7]; Pablo Daniel Ribotta[1,2,3]; Marcela Lilian Martínez[2,3,4]*

[1]Instituto de Ciencia y Tecnología de los Alimentos Córdoba (ICYTAC – CONICET), Universidad Nacional de Córdoba, Córdoba, Argentina.
[2] Instituto de Ciencia y Tecnología de los Alimentos (ICTA), Facultad de Ciencias Exactas, Físicas y Naturales, Universidad Nacional de Córdoba, Córdoba, Argentina.
[3] Departamento de Química Industrial y Aplicada, Facultad de Ciencias Exactas, Físicas y Naturales, Universidad Nacional de Córdoba, Córdoba, Argentina.
[4] Instituto Multidisciplinario de Biología Vegetal (IMBIV, CONICET), Universidad Nacional de Córdoba, Argentina.
[5]Instituto de Investigación y Desarrollo en Ingeniería de Procesos y Química Aplicada (IPQA, CONICET), Universidad Nacional de Córdoba, Argentina.
[6]Grupo de Proteínas Vegetales, Instituto de la Grasa, Consejo Superior de Investigaciones Científicas (CSIC), Sevilla, Spain.
[7]Unidad de Cultivos Celulares, Instituto de la Grasa, Consejo Superior de Investigaciones Científicas (CSIC), Sevilla, Spain.
[8]Grupo de Investigación Ciencia y Tecnología de Sistemas Dispersos, Departamento de Ingeniería Química, Facultad de Química, Universidad de Sevilla, Sevilla, Spain.

*Corresponding author. IMBIV, CONICET, Universidad Nacional de Córdoba, Av. Vélez Sársfield 1611, 5000 Córdoba, Argentina; e-mail address: marcelamartinez78@hotmail.com, marcela.martinez@unc.edu.ar.

E-mail addresses: maria.gabriela.bordon@mi.unc.edu.ar, gabrielabordon90@gmail.com (M.G. Bordón); nalasino@gmail.com (N.P.X. Alasino); alvarovillanueva@ig.csic.es (A. Villanueva-Lazo); cecilio@us.es (C. Carrera-Sánchez); j.pedroche@csic.es (J. Pedroche-Jiménez); mcmillan@ig.csic.es (M.C. Millán-Linares); pribotta@agro.unc.edu.ar (P.D. Ribotta).

Graphical abstract

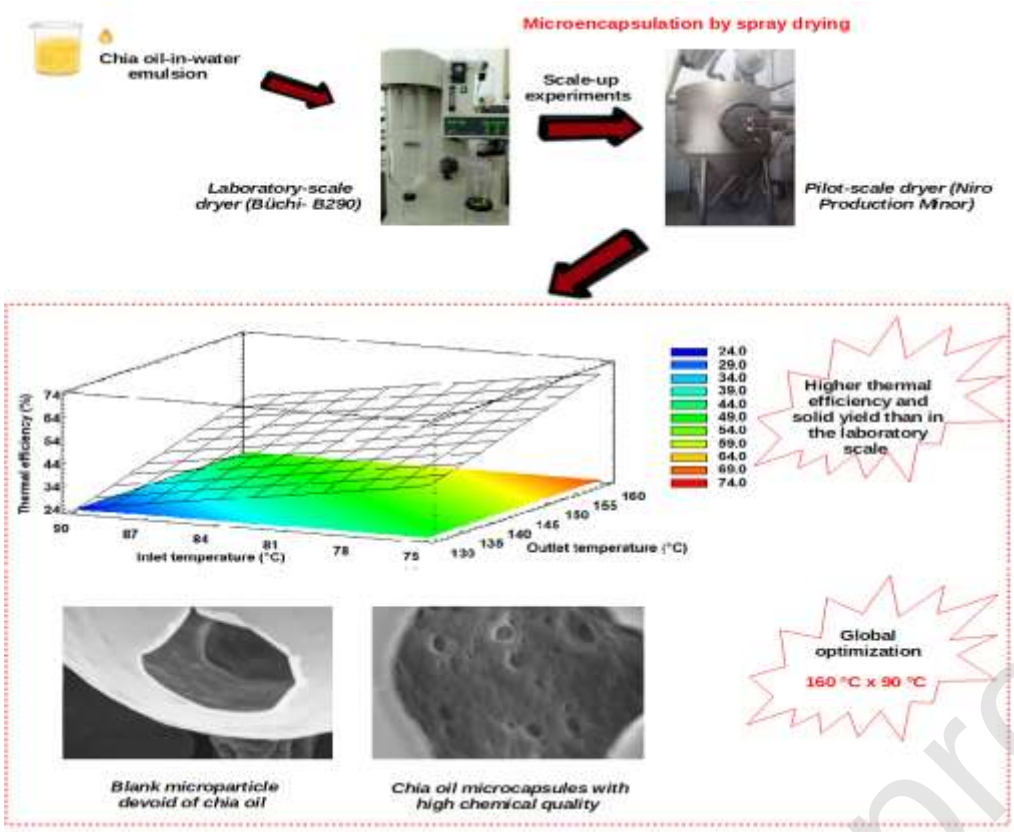

Highlights

- Chia oil quality was preserved by encapsulation in a pilot-scale spray-dryer.
- Higher solid yield (>70%) and thermal efficiency (up to 73%) than in lab-scale process.
- Higher encapsulation efficiency (>90%) than in lab-scale process.
- Enhanced flowability of powders was observed (% compressibility<19%).
- A multiple-response optimization study for pilot-scale spray-drying was performed.

Abstract

A factorial design was performed for the microencapsulation of chia oil by spray drying at pilot-scale, to validate the results obtained previously at laboratory scale in a Büchi-B290. The effects of drying-air inlet (T_{inlet}) and outlet (T_{outlet}) temperatures in a Niro Production Minor on the solid yield, thermal efficiency, theoretical droplet evaporation times, and physico-chemical properties of powders were analyzed. The theoretical droplet evaporation times (0.31-0.54 s) were calculated considering the constant and falling rate periods and a negligible relative velocity between spray and air. Critical diameters between 31.77-41.57 µm were estimated for microcapsules, depending on the process conditions. After scale-up of the spray drying operation, higher solid yields (74.24-79.79%), thermal efficiencies (27.56-73.19%), encapsulation efficiencies (96.97-98.57%), and enhanced flowability of products, compared with experiments at laboratory scale, were observed. Moreover, the scale-up did not affect the chemical composition of microencapsulated oils, their fatty acid composition before and after *in-vitro* digestion processes A global optimization was performed at pilot-scale and the process conditions that simultaneously optimized all the responses was 160 °Cx90 °C (T_{inlet}xT_{outlet}).

Abbreviations

a centrifugal acceleration of the wheel ($m.s^{-2}$)

a^* redness-greenness coordinate

AAD absolute average deviation

A_f accuracy factor

AG arabic gum

AO bioaccessible oil after *in vitro* digestion (%, dry basis)

a_W water activity

b^* yellowness-blueness coordinate

B_f bias factor

C parameter of the GAB model

C_{feed} concentration of dry solids in the feed (kg dry solids/m^3)

CI Carr's Index

CO chia oil

Cp specific heat capacity (J/kg.K)

d wheel diameter (m)

d_i individual desirability

d_{50}^* normalized value of the median ($D_{v,\,0.5}$) diameter

D_O overall desirability function

D_c criticaldroplet/particle diameter (μm)

D_{95} diameter (surface-weighted distribution) below which 95% of the size distribution lies.

$D_{v,\,0.5}$ median of the volume-weighted size distribution (μm)

D [3,2] Sauter mean diameter (μm)

D [4,3] de Broucker mean diameter (μm)

E relative average deviation modulus

E_a activation energy for oxidation reactions (kJ/mol)

E_C evaporative capacity of the dryer (kg/h)

ΔH_{vap} vaporization enthalpy of water (kJ.kg^{-1})

ΔTmean temperature difference between the droplet surface and surrounding air

EE encapsulation efficiency (%, dry basis)

*F*mass flow rate (kg.h^{-1})

*F'*mass flow rate on a dry basis (kg.h^{-1})

h enthalpy of dry solids in the feed (J/kg dry solids)

H enthalpy of dry air (J/kg dry air)

$h_w$wheel vane height (m)

h_c convective heat transfer coefficient (kW.m^{-2}.K^{-1})

HR Hausner ratio

IT induction time (h)

k_d average thermal conductivity of gaseous film surrounding a droplet (kW.m^{-1}.K^{-1})

K_g parameter of the GAB model

L total length of the detachment lines in the atomizer (m, $L = n°h$)

*L** lightness coordinate

MAE mean absolute error

MC moisture content (%, w.b)

MD maltodextrin

N wheel speed (rpm)

N^o number of threads formed at the detachment edge in the atomizer

n^o number of vanes in the atomizer

Nu Nusselt number

PDI polydispersity index

R^2 determination coefficient

SEE standard error of estimates

SOC surface oil content (%, dry basis)

SPI soy protein isolate

SY solid yield (%, dry basis)

t_{cr} drying time corresponding to the constant rate period (s)

t_{dr} droplet evaporation time (s)

t_{EXP} additional exposure time of dry particles (s)

t_{fr} drying time corresponding to the falling rate period (s)

$t_{res,\ a}$ average residence time of air (s)

$t_{res,\ p}$ average residence time of particles (s)

T_{inlet} air inlet temperature (°C)

T_{onset} onset temperature (°C) for oxidation reactions (DSC)

T_{out} air outlet temperature (°C)

T_{wb} wet bulb temperature (°C)

T_{feed} feed inlet temperature (°C)

TOC total oil content of microcapsules (%, dry basis)

V_{feed} feed volumetric flow rate ($mL.min^{-1}$)

V_{th} feed volumetric flow rate per thread in the atomizer ($mL.min^{-1}$)

V_{th}* non-dimensional flow rate per liquid thread in the atomizer

w mass of water (kg)

W moisture content on dry basis (kg water/kg dry solid)

WI whiteness index

W_m monolayer content (kg water/kg dry solids) of the GAB model

Y absolute humidity of air (kg water/kg dry air)

Greek symbols

γsurface tension (dynes.cm^{-1})

η_T thermal efficiency (%)

ρdensity (kg.m^{-3})

Subscripts

1 initial

2 final

c critical point

w.b wet basis

Keywords: Chia oil microencapsulation; spray drying; scale-up; theoretical constant and falling rate periods; critical diameter estimation; optimization.

1 Introduction

Chia (*Salvia hispanica* L.) oil (CO) represents the most abundant vegetable source of omega-3 fatty acids (Bodoira et al., 2017). Despite the health benefits associated with a regular consumption of omega-3-rich oils, the polyunsaturated structure of fatty acids makes this oil highly susceptible against oxidation (González et al., 2021; Punia et al., 2019). Several technological strategies have been applied to stabilize chia oil: addition of natural or synthetic antioxidants (Bodoira et al., 2017), oil blending (Bordón et al., 2019; Guiotto et al., 2014) and microencapsulation in different biopolymer matrices (Copado et al., 2019; Julio et al., 2019; Rodríguez et al., 2019).

Different research articles regarding chia oil microencapsulation by different methodologies can be found in the open literature. Regarding chia oil encapsulation by spray-drying, the following studies during the last five years can be mentioned as examples: Alcântara et al. (2019); Amaya Cano et al. (2021); Copado et al. (2019, 2021); Escalona-García et al. (2016); González et al. (2016); Lavanya et al. (2020); Noello et al. (2016); Santos Fernandes et al. (2021); Timilsena et al. (2016); Us-Medina et al. (2018). Among the available methodologies, spray-drying is probably the most attractive given its simple and continuous operation, the existence of diverse equipment types, and the relatively low production costs (Anandharamakrishnan & Ishwarya, 2019). To the best of the authors' knowledge, there are no reports neither on the scale-up of the drying process nor on the use of pilot-scale spray dryers (more specifically, a Niro Production Minor™, GEA Niro, Søborg, Denmark) for the microencapsulation of chia oil. Previously, our research group studied and optimized the spray drying processes of different chia oil-in-water emulsion formulations in two smaller-scale spray dryers: a Mini Spray Dryer Büchi B-290 (Büchi Labortechnik AG, Flawil, Switzerland) and a Niro Mobile Minor (GEA Niro, Søborg, Denmark) (Bordón et al., 2021a,b). Hence, the main scientific contribution of the present research was based on the scale-up (from previous experiences at the laboratory-scale) and optimization of the spray-drying process at pilot-scale for the microencapsulation of chia oil, in order to validate the results and the global optimum found previously by our research group with a laboratory-scale dryer. The optimization study at pilot-scale

was performed in a Niro Production Minor™ dryer, involving not only an exhaustive physicochemical characterization of the products obtained, but also important process variables, such as the solid yield, the thermal efficiency of the dryer, a theoretical droplet evaporation time and a theoretical residence time of particles within the hot environment of the dryer's chamber.

The main goal for the scale-up of spray-drying processes is to increase the production rate and yield, while preserving specific properties of powders across scales (Poozesh & Bilgili, 2019). The chemical quality of chia oil must be preserved after the scale-up of the drying operation. With that aim, a sound understanding and characterization of a smaller-scale spray-drying process that yields products with acceptable physicochemical properties is a prerequisite. According to Bordón et al. (2021b), the chemical quality of microencapsulated chia oil was significantly damaged during drying in the Niro Mobile Minor, possibly due to the contact of product with hot air caused by back-mixing around a central air disperser, and the extended residence time in the chamber. Indeed, these recirculation zones are described by Masters (1979) as local areas of counter-current flow between the main air stream and the product. Hence, the product is carried to the hottest-air zones; its residence time in the chamber is increased, as well as the damage to the heat-sensitive product.Nonetheless, the oil was successfully protected by the process carried out in the Büchi B-290, in which plug-flow conditions prevailed. Therefore, the thermodynamic design space and the optimum process conditions established for the microencapsulation of chia oil in this latter dryer were the basis for the scale-up in the present analysis. The thermodynamic design space is the operation range over which the desired outlet conditions in the spray dryer are attainable. This space is defined by simplified mathematical models that entail easily measured process variables: feed, drying-air and atomizing-air flow rates, drying-air inlet and outlet temperatures, and relative humidity at the outlet of the drying chamber (Poozesh & Bilgili, 2019).

In the precedent optimization studies published by our group, a theoretical droplet evaporation time was analyzed as a response variable to minimize, given that the losses of heat-sensitive products during drying are dictated by the drying kinetics, the air temperature and the particle flow (Schmitz-Schug et al., 2013). However, only the constant rate period was considered in a simplified approach, based on Lisboa et al. (2018). Hence, it becomes necessary to estimate the complete droplet evaporation time by considering both the constant and falling rate periods, and by means of a simple model.

Based on the above context, the objectives of this research were: 1) to study the influence of drying air inlet (T_{inlet}) and outlet (T_{outlet}) temperatures in a pilot-scale dryer on the solid yield, the thermal efficiency, and the physicochemical properties of microencapsulated chia oil; 2) to estimate a theoretical time necessary to dry a single droplet of chia oil-in-water emulsion, by considering both the constant and falling rate periods; 3) to optimize the spray-drying process at pilot-scale for the microencapsulation of chia oil; 4) to understand the effect of the incorporation of the core material (chia oil) on the microstructure and properties of powders obtained at pilot-scale.

2 Materials and methods

2.1 Materials

Chia seeds were obtained from Cartago Group (Spain). The oil was obtained by solid-liquid extraction with *n*-hexane during 24 h in an Armfield FT29 extractor (England) at room temperature. The solvent was then evaporated in a rotary evaporator at 37 °C (Büchi Labortechnik, Switzerland). Soy protein isolate (SPI) EXPRO™ 510A with 90 % protein (fat-free, dry basis) was obtained from Singlory Health Food (Portugal); arabic gum (AG) and maltodextrin (MD) were purchased to Roquette (Spain); *n*-hexane, petroleum ether, citric acid, sodium hydroxide and sodium chloride were of

analytical grade (PanReac, AppliChem, ITW reagents, Iberia); alpha-amylase, pepsin and pancreatin were obtained from Sigma Aldrich (USA).

2.2 Preparation of blank dispersions and O/W emulsions

SPI and AG powders were redispersed in Milli-Q water for 1 h according to Bordón et al. (2021a,b). The necessary quantity of powder to obtain a total biopolymer concentration of 12 % (w/v) and a 1/1 SPI/AG ratio (w/w) was weighed. The blank dispersions (without chia oil) and the O/W emulsions were prepared following the procedure by Bordón et al. (2021a,b) with brief modifications. The composition of both preparations is shown in **Table 1**. SPI and AG dispersions were blended with a high speed homogenizer (9000 rpm, 2 min, Ultraturrax IKA T50, Germany). Afterward, CO was gently incorporated drop-wise into the SPI+AG suspension by high speed homogenization (2 min, 9000 rpm). The coarse emulsions were homogenized for 1 cycle at 700 bars in a high pressure valve homogenizer (EmulsiFlex C-5, Avestin, Canada). The pH of the fine emulsions was adjusted to 3.00 with 2 M citric acid in order to induce the complex coacervation reaction between SPI and AG. The reaction medium was stirred during 30 min in a 25 L-stirred tank reactor; the carrier agent (MD, 4 % w/v) was incorporated during stirring, before spray-drying. Finally, 5 L-batches of blank dispersions or emulsions were spray dried in triplicate.

2.3 Spray-drying device and experimental design

2.3.1 Spray-drying device

Pilot-scale drying experiments were performed in a co-current short-type spray dryer, the Niro Production Minor™. The aspect ratio (height/diameter) and the surface area are 1.78 m/1.20 m and 6.20 m^2, respectively. The dryer is equipped with a 0.1 m-diameter rotary wheel atomizer (24 straight vanes, 0.0055 m-height).

In this dryer, the desired drying-air inlet temperature is obtained by adjusting the heater system. When an outlet air temperature of approximately 120 °C has been reached during start up (advised by the manufacturer), water is slowly led to the atomizer by manual regulation of the speed of the feed pump. The desired drying-air outlet temperature is obtained by the amount of water introduced. When both the inlet and outlet air temperatures are stable on the required and programmed values, the change over from water to product can take place and the feed pump is regulated automatically. As can be seen, the feed pump can be regulated manually or automatically. When starting up the process, manual regulation is recommended by the manufacturer. At a stabilized temperature profile, the user can switch from manual to automatic control and the feed flow rate is controlled by means of the drying-air inlet and outlet temperatures thereafter.

2.3.2 Spray-drying experimental design

Spray-drying scale-up can be more challenging than for other unit operations, since drying generally exerts a greater influence on the products' properties than other unit operations, for instance, density, particle size, wettability, flowability, flavor, color, among others (Masters, 1979). Therefore, a complete characterization of the powders obtained with a smaller-scale spray dryer is a necessary starting point to identify the key particle properties across scales (Al-Khattawi et al., 2018).

Design of experiments (DOE) studies performed on the small scale help define the critical process parameters, which would then be considered during the scale-up experiments. However, the design space created on the smaller scale may not always be applicable to the larger scales due to differences in initial atomized drop size, tower designs, residence

times, etc. Consequently, a common practice is to validate the design space upon scale-up (Al-Khattawi et al., 2018). With the aim of re-validating the design and results observed previously with the same emulsion formulation, spray dried at laboratory-scale in the Büchi-B290 according to Bordón et al. (2021b), a multilevel factorial design was performed at larger scale in the Niro Production Minor™. The effects of T_{inlet} and T_{outlet} asexperimental factors on the response variables described in sections 2.3.4.1 to 2.3.4.4.7 were analyzed. Moreover, other processing conditions, besides T_{inlet} and T_{outlet}, are listed in **Table 1**. The experiments were randomized and carried out in triplicate.

The chemical quality of microencapsulated chia oil is a target property to preserve across different scales. According to the results observed with the Büchi-B290, the oxidative stability index (Rancimat test) decreased significantly ($p \leq 0.05$) from 6.33-6.42 h to 5.14-5.42 h with the increase in the drying-air inlet temperature (T_{inlet}) from 130-160 to 190 °C, respectively. Therefore, an inlet temperature of 190 °C was not evaluated in the scale-up experiments of this research. In addition, the drying-air outlet temperatures (T_{outlet}) for 130-160 °C were between 70-90 °C in the Büchi-B290. Hence, similar drying air temperatures should be achieved at a larger scale. After identifying the target properties of powders and the range of drying-air temperature, a standard method of scale-up in industry (by users and manufacturers) was followed in the present study. It consists of scaling the spray rate proportionately to the maximum processing drying air flow rate (Kemp, 2017). The aim is to maintain T_{outlet} between scales with modest adjustments of T_{inlet}. The approach allows users to keep the final moisture content of products and the outlet relative humidity similar across scales as well (Poozesh & Bilgili, 2019).

Multifactorial ANOVA procedures in STATGRAPHICS® (Statpoint Technologies, Warrenton, VA, USA) were applied to evaluate the statistical significance ($p \leq 0.05$) of T_{inlet}, T_{outlet} and their interaction on the dependent variables. Linear or quadratic polynomial models were fitted, which assume the following form according to the levels of the experimental factors studied:

$$Y' = \beta_0 + \beta_1 X_1 + \beta_2 X_2 + \beta_{12} X_1 X_2 \quad \textbf{(Eq. 1)}$$

where Y' is the modeled dependent variable, β_0, β_i and β_{ij} are the constant term, the linear and interaction coefficients, respectively; $X_1$and X_2 are$T_{inlet}$and T_{outlet}, respectively.

The regression models were evaluated according to the determination coefficient (R^2), the standard error of estimates (*SEE*) and the mean absolute error (*MAE*). As long as a direct experimental validation could be performed, the relative deviation between predicted and observed responses was also assessed. Hence, the absolute average deviation (*AAD*), the accuracy factor (A_f) and the bias factor (B_f) were estimated as described Desobgo et al. (2015):

$$AAD = \left[\sum_{i=1}^{n} \left|Y_{i,e} - Y'_i\right| / Y_{i,e}\right] / n \quad \textbf{(Eq. 2a)}$$

$$B_f = 10^{\frac{1}{n}\sum_{i=1}^{n} log\left(\frac{Y'_i}{Y_{i,e}}\right)} \quad \textbf{(Eq. 2b)}$$

$$A_f = 10^{\frac{1}{n}\sum_{i=1}^{n} \left|log\left(\frac{Y'_i}{Y_{i,e}}\right)\right|} \quad \textbf{(Eq. 2c)}$$

where Y'_i, $Y_{i,e}$ and n are the predicted and observed values of the responses and the number of experiments, respectively.

2.3.3 Volumetric feed rate and non dimensional flow rate per liquid thread

The volumetric feed rate (V_{feed}) was directly read (mL/min) during each experimental run, from the pump display after switching from manual to automatic control (section 2.3.1). From V_{feed}, the non dimensional flow rate per liquid thread (V_{th}*) was calculated (**Eq. 3**). In rotary atomizers, a minimum value between $1<V_{th}*<1.5$ should be overcome to obtain liquid threads at equal intervals along the circumference of the atomizer (Walzel, 2012). A uniform distribution of the feed on the vanes allows a homogeneous size distribution of atomized droplets (Masters, 1979).

$$V_{th}* = V_{th.}(a^3.\rho_{feed}^5/\gamma^5)^{1/4} \quad \textbf{(Eq. 3)}$$

where a is the centrifugal acceleration of the wheel (a= 3.42 x 10^5 m.s^{-2}), ρ_{feed} is the density and γ is the surface tension of the feed, for which the values at 25 °C were determined according to Bordón et al. (2021a) and were 1003.00±0.00 kg.m^{-3} and 48.86±1.41 dynes.cm^{-1}, respectively; V_{th} is the flow rate per thread ($V_{feed}/N°$) and N^o is the number of threads ($N^o = (L/7)(\rho_{feed}.a/\gamma)^{1/2}$); L is the total length of the detachment lines ($n°h$), and $n°$ and h are the number and height of the vanes, respectively (Walzel, 2012).

2.3.4 Response variables for global optimization

The response variables described below were considered essential for a global optimization based on a more efficient drying process (solid yield, thermal efficiency and additional exposure time of dry microcapsules in the chamber) and on critical quality attributes (CQAs) of the obtained microcapsules that preserve the functionality of the encapsulated oil. The CQAs are usually identified as physical, chemical, biological or microbiological properties or characteristics that should be within a defined range to ensure the product quality, safety and efficacy (Charoo et al., 2012). For chia oil microcapsules, the identified CQAs are described in section 2.3.4.4: the water activity, moisture content, the mean diameter of particles, the normalized median diameter of oil droplets in reconstituted emulsions, color (whiteness index), flow properties (Carr's Index and Hausner ratio), encapsulation efficiency, the bioaccessible oil, and the chemical quality (oxidative stability index).

2.3.4.1 Solid yield

The solid yield (SY) was determined immediately after the end of each experiment, and was calculated by dividing the final powder weight (dry basis) and the dried weight of solid components in the feed (Bordón et al., 2021a).

2.3.4.2 Thermal efficiency

The thermal efficiency (η_T) of a dryer is defined as the ratio of the heat used in the evaporation and the heat input (Masters, 1979). If the heat losses cannot be neglected during operation, the following equation should be used (Bhandari et al., 2008):

$$\eta_T = \frac{E_C \Delta H_{vap}}{F_{dryingair} Cp_{dryingair}(T_{inlet} - T_{wb}) + F_{feed} Cp_{feed}(T_{feed} - T_{wb})} \quad \textbf{(Eq. 4)}$$

where E_C is the evaporative capacity of the dryer (kg/h), ΔH_{vap} is the enthalpy of vaporization of the solvent (kJ/kg) (**Appendix A.1**); $F_{drying\ air}$ and F_{feed} are the mass flow rates of the drying-air and the feed, respectively (kg/h); T_{wb} and T_{feed} are the wet bulb temperature corresponding to T_{inlet} and the inlet temperature of the feed, respectively (°C); $Cp_{drying\ air}$ and Cp_{feed} are the specific heat capacities of the drying air and the feed, respectively (kJ/kg.K) (**Appendixes A.2.1** and **A.2.2**).

2.3.4.3 Estimation of a single droplet evaporation time and additional exposure time of dry microcapsules in the chamber

2.3.4.3.1 Single droplet evaporation time

The estimation of a droplet evaporation time (t_{dr}) was based on a fundamental model, according to Martínez (2009) with brief modifications. The set of equations (equations **5-24**) will be referred as drying kinetic model thereafter. The set of equations were solved with MATLAB programming (Math Works Inc., Natick, MA, USA).

The model may be applied to pure liquid droplets, as well as to suspensions because of the negligible vapor-lowering effects in droplets containing insoluble solids (Masters, 1979). Other assumptions or simplifications may be summarized as follows: drying of spherical droplets; the shape of the droplets does not change during drying; collisions and agglomeration between droplets/particles are ignored; negligible relative velocity conditions between the evaporating droplet and drying air. This last assumption is based on the fact that a droplet is completely influenced by the air flow during the greatest part of its trajectory. Hence, the heat transfer to a spherical droplet through still air is expressed as Nu = 2.0 (Masters, 1979). Finally, the estimations were based on the drying of a droplet whose initial diameter equals the D_{95} diameter ($D_{95,1}$, surface-weighted distribution), below which 95% of the size distribution of the spray lies. If such a droplet is dried before it hits the chamber wall, then 95 % of the atomized spray will be dried as well (Martínez, 2009).

The total evaporation time (t_{dr}) was calculated as the sum of the times for the constant (t_{cr}) and falling rate (t_{fr}) periods. The drying time corresponding to the constant rate period (t_{cr}) was calculated with **Eq. 5**, whose deduction can be found in Bordón et al. (2021a,b). It is based on the assumption of dynamic equilibrium, where the rate of heat transfer equals the product of the rate of mass transfer from a saturated surface and the latent heat of vaporization. The constant rate period ends when the droplet/particle reaches its critical diameter (D_C), as surface wetness can no longer be maintained (Masters, 1979).

$$t_{cr} = \frac{\Delta H_{vap}\rho_{droplet}\left(D_{95,1}^2 - D_c^2\right)}{8k_d\Delta T_1} \textbf{(Eq. 5)}$$

where $\rho_{droplet}$ is the density of the droplet (kg/m^3), which is equal to ρ_{feed}; D_C is the critical diameter; k_d is the average thermal conductivity of the air film surrounding a droplet (**Appendix A.3**); ΔT_1 is logarithmic mean temperature difference between the droplet surface and the surrounding air.

The $D_{95,1}$ diameter of the spraying Eq. 5 was estimated from its Sauter mean diameter (D [3,2]). The following correlations for rotary atomizers were used:

$$D[3,2] = \frac{1.4x10^4(F_{feed})^{0.24}}{(Nd)^{0.83}(n^o h_w)^{0.12}}$$(Masters, 1979) (**Eq. 6**)

where 1.4 x 10^4 is an empirical constant; F_{feed} is the mass flow for the feed (kg/h); N is the wheel speed (rpm), d is the wheel diameter (m), n^o is the number of vanes and $h_w$is the vane height (m).

$D_{95,1}$ = 1.4 D *[3,2]* (Martínez, 2009) (**Eq. 7**)

The critical diameter D_C in Eq. 5can be deduced from a mass balance of dry solids in a droplet/particle, from the inlet to the exit of the drying chamber (**Eq. 8**). Assuming no droplet collisions, the mass of dry solids is constant.

$$\frac{v_1\rho_{droplet}}{1+W_1} = \frac{v_2\rho_{particle}}{1+W_2}$$(**Eq. 8**)

where v_1 and v_2 are the initial and final droplet/particle volume, respectively; $\rho_{particle}$ is the density of the final particle; W_1 and W_2 are the initial and final moisture contents on a dry basis (kg water/kg dry solids).

The density of the final particle ($\rho_{particle}$) was calculated according to Langrish (2009):

$$\rho_{particle} = \frac{1+W_2}{1+W_2\frac{\rho_{drysolid}}{\rho_{water}}}\rho_{drysolid}$$(**Eq. 9**)

where $\rho_{dry\ solid}$ is the density of dry solids, which can be calculated with an expression similar to Eq. A4 in Appendix A. Expressions for the density of each component of the feed (moisture, lipids, protein, carbohydrates and ash) can be found in Shamaei et al. (2017).

It was assumed that once the critical point was reached, the particle diameter remained constant (D_C) until the exit (Martínez, 2009). Replacing the volumes in **Eq. 8** for the volume of a sphere:

$$\frac{\frac{4}{3}\pi\frac{D_{95,1}^3}{8}\rho_{droplet}}{1+W_1} = \frac{\frac{4}{3}\pi\frac{D_C^3}{8}\rho_{particle}}{1+W_2}$$(**Eq.10**)

from which D_C (Eq.5) can be obtained:

$$D_C = D_{95,1}\left(\frac{\rho_{droplet}}{\rho_{particle}}\frac{1+W_1}{1+W_2}\right)^{1/3}$$ (**Eq. 11**)

The logarithmic mean temperature difference ΔT_1 can be calculated as follows (Masters, 1979):

$$\Delta T_1 = \frac{(T_{inlet}-T_{feed})-(T_{dryingair,c}-T_{feed,c})}{log\left(\frac{T_{inlet}-T_{feed}}{T_{dryingair,c}-T_{feed,c}}\right)}$$(**Eq. 12**)

where the subscript 'c' refers to the critical point.

In Eq. 12, the temperature of a droplet composed of suspensions is equal to the wet-bulb temperature of air during the

constant rate period. Therefore, when it reaches the critical point:

$T_{feed,c} = T_{wb}$ (**Eq. 13**)

The absolute humidity of drying air (Y_C) at the critical point can be estimated from a global mass balance according to Martínez (2009), from the inlet of the drying chamber to the critical point:

Global mass balance:

$$F'_{feed}(W_1 - W_C) = F'_{dryingair}(Y_C - Y_1) \text{(Eq. 14)}$$

where F'_{feed} and $F'_{drying\ air}$ are the feed and drying air mass flow rates on a dry basis (kg/h), Y_1 is the inlet absolute humidity of drying air (kg water/kg dry air).

The moisture content of the feed at the critical point on a dry basis (W_c) that appears in Eq. 14 was calculated from the mass of water removed ($w_{removed}$) from the droplet when it reaches the critical point:

$$w_{removed} = \frac{\pi}{6}\left(D_{95,1}^3 - D_C^3\right)\rho_{water} \text{(Eq. 15)}$$

Mass of remaining moisture:

$$w_{remaining} = \frac{\pi}{6} D_{95,1}^3 W_{1,w.b}\rho_{droplet} - w_{removed} \text{(Eq. 16)}$$

where $W_{1,w.b.}$ is the moisture content of the feed on a wet basis (kg water/kg wet solids), which can be calculated from the moisture content on a dry basis as ($W_{1,w.b.} = W_1/(1+W_1)$) (Treybal, 1980).

Therefore,

$$W_C = \frac{w_{remaining}}{\left(\frac{\pi D_{95,1}^3}{6} C_{feed}\right)} \text{(Eq. 17)}$$

where C_{feed} is the concentration of dry solids in the feed (kg dry solids/m^3), which can be estimated as $C_{feed} = (1-W_{1,w.b})\rho_{feed}$ (Martínez, 2009).

From Eq. 17, and the known variables F'_{feed}, $F'_{drying\ air}$, W_1 and Y_1, Y_C can be calculated.

The temperature of drying-air ($T_{drying\ air,c}$) (Eq.12) at the critical point can be estimated from a global energy balance according to Martínez (2009), from the inlet of the drying chamber to the critical point:

Global energy balance:

$$F'_{feed}(h_1 - h_C) = F'_{dryingair}(H_C - H_1) \text{(Eq. 18)}$$

where h_1 and H_1 are the inlet enthalpies of the solids in the feed and of the dry air (J/kg), respectively; h_c and H_C are the enthalpies of the solids in the feed and of the dry air in the critical point, respectively.

In addition,

$$h_1 = Cp_{drysolid}\left(T_{feed} - T_{ref}\right) + W_1 Cp_{water}\left(T_{feed} - T_{ref}\right) \textbf{(Eq. 19)}$$

where T_{ref} is a reference temperature (0 °C).

$$h_C = Cp_{drysolid}\left(T_{feed,c} - T_{ref}\right) + W_C Cp_{water}\left(T_{feed,c} - T_{ref}\right) \textbf{(Eq. 20)}$$

The enthalpies of dry air were calculated according to Langrish (2009):

$$H_1 = (1.005 + 1.880Y_1)\left(T_{inlet} - T_{ref}\right) + \Delta H_{vap} Y_1 \textbf{(Eq. 21)}$$

$$H_c = (1.005 + 1.880Y_c)\left(T_{dryingair,c} - T_{ref}\right) + \Delta H_{vap} Y_C \textbf{(Eq. 22)}$$

Then $T_{drying\ air,\ c}$ is obtained from Eq. 22.

Finally, the drying time corresponding to the falling rate period (t_{fr}) was calculated with Eq.23, which can be found in Masters (1979):

$$t_{fr} = \frac{\Delta H_{vap} D_C^2 \rho_{drysolid} (W_C - W_2)}{12 k_d \Delta T_2} \textbf{(Eq. 23)}$$

The logarithmic mean difference temperature ΔT_2 was estimated as follows:

$$\Delta T_2 = \frac{\left(T_{dryingair,c} - T_{feed,c}\right) - \left(T_{outlet} - T_{particle,outlet}\right)}{log\left(\frac{T_{dryingair,c} - T_{feed,c}}{T_{outlet} - T_{particle,outlet}}\right)} \textbf{(Eq. 24)}$$

where the outlet temperature of dry particles $T_{particle,outlet}$ was supposed to be approximately 20 °C lower than T_{outlet} according to Anandharamakrishnan & Ishwarya (2015).

2.3.4.3.2 Additional exposure time of dry microcapsules

The additional exposure time of dry particles in the dryer (t_{EXP}) was estimated as the difference between the average residence time of the particle in the dryer ($t_{res,p}$) and the droplet evaporation time t_{dr} (Bordón et al., 2021b). Two assumptions or simplifications were considered. First, the residence time was longer than the evaporation time, which means that drying of droplets was completed before the final dry particle exits the dryer (Kemp et al., 2016). Second, the minimum residence time of the particle was equal to the average residence time of the drying air (Masters, 1979). Assuming plug flow conditions, the average residence time for the drying air was estimated as the ratio of the chamber volume and the air volumetric rate (evaluated at the outlet temperature and relative humidity) (Masters, 1979).

2.3.4.4 Physicochemical properties of chia oil microcapsules

2.3.4.4.1 Water activity and moisture content

Water activity at 25 °C (a_W) was determined as described by Bordón et al. (2021b), using an Aqua-Lab Water Activity Meter (208 Series 3, Decagon Devices Inc., USA). Moisture content (*MC*) was measured following the methodology given by González et al. (2016) and expressed as g/100 g wet product (%, wet basis).

2.3.4.4.2 Size distribution of powders and normalized value of the median diameter (d_{50}*) for oil droplets in reconstituted emulsions

The size distribution, mean particle diameters (D [4,3] or de Brouckere and D [3,2] or Sauter diameters) and the polydispersity index (PDI) of powders were determined by laser diffraction with an HORIBA analyzer (LA 950V2 model, Japan) at 25 °C, according to Di Battista et al. (2017). A relative refractive index of 1.01 and an absorption value of 0.1 were used in the calculations.

Changes in the oil droplet size distribution of emulsions have been reported to take place during rotary atomization, shifting the original distribution to larger diameter values due to the velocity gradients applied to the feed (Bordón et al., 2021a; Munoz-Iibanez et al., 2015). The impact of atomization on the original (or parent) emulsion structure was assessed considering the volume median diameter ($D_{V,0.5}$) of oil droplets as a characteristic length, and with the aim of compensating the difference in the initial $D_{V,0.5}$ of different emulsions, a normalized d_{50}* value was calculated as proposed by Munoz-Ibanez et al. (2015):

$$d_{50}* = \frac{D_{V,0.5}[reconstitutedemulsion]}{D_{V,0.5}[parentemulsion]} \quad \textbf{(Eq. 25)}$$

where 50% of the oil volume in a parent or a reconstituted emulsion is contained in oil droplets of diameter below or equal to the median value $D_{V,0.5}$ (Julio et al., 2018).

For the above calculation, the powders were first dispersed in distilled water (10 g solids/100 mL emulsion) and subsequently vortexed (3 x 2 min) according to Bordón et al. (2021a,b). A relative refractive index of 1.10 and an absorption value of 0.1 were used (Julio et al., 2018).

2.3.4.4.3 Color

The color of powders was measured following the methodology of González et al. (2016) and expressed as a whiteness index (*WI*) based on Rodríguez et al. (2019). *WI* was calculated from the CIELAB coordinates:

$$WI = L* - 3b* \quad \textbf{(Eq. 26)}$$

2.3.4.4.4 Flow properties

The powder flowability was assessed by the Carr's Index (*CI*) or "percent compressibility" and the Hausner ratio (*HR*), both determined and calculated based on Rodríguez et al. (2019). Briefly, around 25 g (m_0) of each sample was poured through a funnel into a 100 mL-glass graduated cylinder. The volume (v_0) occupied was read directly from the cylinder to calculate the aerated density ($\rho_A = m_0/v_0$). The cylinder was then tapped until a constant volume (v_T) was reached, in

order to calculated the tapped density ($\rho_T = m_0/v_T$). The *CI* and *HR* were estimated as follows:

$$CI = \left(\frac{\rho_T - \rho_A}{\rho_T}\right) x100 \textbf{(Eq. 27)}$$

$$HR = \frac{\rho_T}{\rho_A} \textbf{(Eq. 28)}$$

2.3.4.4.5 Encapsulation efficiency

Surface oil content (*SOC*), total oil content (*TOC*) and encapsulation efficiency (*EE*) were determined by following the methodologies detailed in Holgado et al. (2019). *EE* was expressed on a dry basis and calculated with the equation:

$$EE = \left(\frac{TOC - SOC}{TOC}\right) x100 \textbf{(Eq. 29)}$$

2.3.4.4.6 Bioaccesible oil after *in-vitro* digestion

With the aim of determining the amount of bioaccessible oil (*AO*) for intestine absorption, an *in vitro* digestion of microcapsules was performed. Two methodologies were followed to prepare a simulated salivary fluid (SSF) (Timilsena et al., 2017), as well as simulated gastric (SGF) and intestinal (SIF) fluids (González et al., 2018). Subsequently, 4 g of microcapsules were subjected to 12.5 mL of SSF (2 min, 37 °C) in an orbital shaker. The pH was adjusted to 2.0 with 1 M HCl and 25 mL of SGF were added. The powders were exposed to SGF during 2 h at 37 °C. Afterward, the pH of the mixture was adjusted to a value of 7.0 with 1 M NaOH and 25 mL of SIF were added and mixed for 2 h at 37 °C (Bordón et al., 2021b).

The lipid compounds were separated from the simulated digestion mixture with *n*-hexane (3 x 50 mL), the solvent was evaporated, and the mass of remaining oil ($m_{oil,2}$) was weighed and compared to the initial mass of oil ($m_{oil,1}$) added to the formulation. The *AO* was estimated as ($AO = (m_{oil,2}/m_{oil,1}) \times 100$) (González et al., 2018).

2.3.4.4.7 Oxidative stability index

The chemical quality of the core was evaluated by the oxidative stability index (OSI) expressed as an induction time (*IT*) in hours. Rancimat analysis was performed for bulk and microencapsulated oils according to Oliveira et al. (2002) (air flow rate: 20 L/h, temperature of the heating block: 100 °C).

2.3.5 Multiple response optimization

Regression models (**Eq. 1**) were fitted for the responses and were combined in an overall desirability function (**Eq. 30**) to establish the optimum process conditions (T_{inlet} x T_{outlet}), which simultaneously optimized all the dependent variables within the explored domain (Di Battista et al., 2017). The optimization goals, which will be highlighted in the Results and Discussion section, depended heavily on the spray-drying process and the identified critical quality attributes of microcapsules (section 2.3.4.4). The overall desirability function (D_o) is:

$$D_0 = (d_i)^{1/r} \textbf{(Eq. 30)}$$

where *r* is the total number of dependent variables and $d_i$is an individual desirability function. This latter varies between 0 (completely undesirable) and 1 (fully desirable). In order to validate the regression models and the optimum conditions found, three independent runs were performed and the experimental responses were determined. Finally, the relative deviation between predicted and observed responses values was calculated, as long as an experimental validation was possible. *AAD*, A_f and B_f were calculated as shown above (**Eqs. 2a** to **2c**).

2.3.6 Additional characterization of microcapsules obtained under the optimum processing conditions

2.3.6.1 Fatty acid profile before and after *in-vitro* digestion

Fatty acid profiles of bulk and microencapsulated oils (before and after *in vitro* digestion) were studied by gas chromatography (Perkin Elmer, Shelton, CT, 201 USA) (Martínez et al., 2017).

2.3.6.2 Differential scanning calorimetry

Differential scanning calorimetry (DSC) experiments (DSC Q20 V24.11 Build 124, TA Instruments, USA) were performed with bulk and microencapsulated oils to evaluate the thermal stability in non-isothermal tests, and under a non-inert atmosphere. Samples were heated in open aluminum holders at three different linear heating rates β(5, 10, and 20 °C/min) from 25 to 350 °C as proposed by Guimarães-Inácio et al. (2018). Kinetic data of oxidation reaction in oils (T_{onset} and E_a) were calculated according to procedures well-described elsewhere (Guiotto et al., 2014; Guimarães-Inácio et al., 2018). The activation energy (E_a, kJ/mol) was calculated as:

$$E_a = -2.19R\frac{dlog\beta}{dT^{-1}} \textbf{(Eq. 31)}$$

$$log\beta = aT^{-1} + b \textbf{(Eq. 32)}$$

where *R* is the gas constant, $T = T_{onset}$ (K), *a*and *b* are the slope and intercept of the Arrhenius plots, respectively (Guiotto et al., 2014).

2.4 Comparison between chia oil microcapsules and blank microparticles

According to the objective number 4) given in section 1, blank dispersions (without chia oil) were prepared and subsequently spray dried (**Table 1**). The blank microparticles obtained were characterized according to sections 2.3.4.4.1 to 2.3.4.4.4. Moreover, with the aim of assessing the stability of redispersed powders and their morphology, the following analysis were also performed:

2.4.1 Back scattering profile after redispersion

In order to study the physical stability, the powders were first redispersed in a similar manner as described in section 2.3.4.4.2. The stability was investigated by measurements of dispersed light according to Julio et al. (2018), using a Vertical Scan Analyzer Quick Scan (Coulter Corp., USA). The sample scans were repeated periodically for 48 h.

2.4.2 Morphology

The morphology was studied by scanning electron microscopy (SEM). Microcapsules and blank microparticles were coated with gold under vacuum, and examined with a FEG SEM scanning electron microscope (Carl Zeiss Sigma, Germany) (González et al., 2016).

2.5 Statistical analysis

All the analytical determinations of this research were the averages of three independent measurements (n=3). The ANOVA test at 5% level of significance ($p \leq 0.05$) was used to assess the statistical differences among treatments for all variables. Whenever the ANOVA indicated a significant difference, a pair-wise comparison of means by the Fisher's least significant difference (LSD) procedure was performed with STATGRAPHICS®.

3 Results and discussion

3.1 Volumetric feed rate and non dimensional flow rate per liquid thread

Table 2 shows the values for the feed rate or V_{feed}, which are important for the time length of the drying operation. In this regard, it should be highlighted the rise in V_{feed} after the scale-up: from 2.8-15 mL/min in smaller-scale dryers (Büchi- B290 and Niro Mobile Minor) (Bordón et al., 2021b) to 64.62-196.09 mL/min (Table 2) in the Niro Production Minor, for the same emulsion formulation. Moreover, there was an increment in V_{feed} as the programmed difference $T_{inlet} - T_{outlet}$ increased. This may be attributed to the fact that, for a given T_{inlet}, more solvent should be evaporated in the chamber to decrease T_{outlet} (Masters, 1979).

Regarding the non dimensional flow rate per thread, Eq. 3 highlights that V_{th}* and V_{feed} are linearly related, which is important for a complete wetting of the vane surface (Masters, 1979). In order to achieve a regular thread formation, at equal intervals along the wheel, not only a complete wetting of the vane surface by a uniform liquid feed rate has to be ensured, but also high peripheral speeds (Masters, 1979; Walzel, 2012). In this research, V_{th}* values above 1.5 (Table 2), and higher than those informed by Bordón et al. (2021b) (between 0.31-0.47), were calculated. This might be due to different reasons; first, the higher V_{feed} processed in a larger-scale dryer; second, the higher centrifugal acceleration in the present study, which in turn was caused by higher revolutions and a larger diameter of the wheel, compared with that of Bordón et al. (2021b)($a = 1.21 \times 10^5$ m.s^{-2}). Finally, the V_{th}* values recorded in this research exerted a great influence on the uniformity of the oil droplet size distribution in reconstituted emulsions after atomization, compared with that of the parent emulsion (section 3.2.4). On the contrary, Bordón et al. (2021b) observed the presence of larger oil droplets and a more heterogeneous distribution after the atomization of emulsions.

3.2 Spray-drying experimental design: Response variables

The regression coefficients, their statistical significance and the goodness-of-fit of the models for the response variables can be found in **Table 3** and **5**.

3.2.1 Solid yield

The solid yield (SY) represents a fundamental variable to analyze, because the scale-up of the drying operations is aimed to maximize the obtainment of dry product by handling higher volumes of the feed in a chamber of larger

dimensions (Al-Khattawi et al., 2018). As can be seen from Table 3 and **Fig.1**, SY values between 70-80 % were obtained, being higher than those informed, for a similar emulsion formulation, by Bordón et al. (2021b)in a smaller-scale dryer, the Niro Mobile Minor (40-46%). The SY range observed in the present study was also above the values reported for chia oil encapsulation by Santos Fernandes et al. (2021), who obtained the microcapsules with a yield of 50%.

It is important to point out that the heat loss from the walls and yield may vary between scales. Particularly, SY on the small-scale dryers are limited to 60-70 % (or below 50% in the worst scenario) due to the presence of fine particles remaining in the filters or due to the formation of wall deposits (Al-Khattawi et al., 2018; Poozesh & Bilgili, 2019). Chamber deposits are prevented, or at least minimized, after scale-up because of the high investments in new spray dryer capacities, which usually involve improved performances to produce better-quality powders while preventing degradation and contamination from deposits, etc. (Masters, 1979). Moreover, the differences in SY may be attributed to the thermal efficiency of the drying process, which is related to the heat input required to produce a unit weight of dry product and varies across scales (Al-Khattawi et al., 2018; Kemp, 2017). The heat losses through the dryer walls tend to be greater in the small scale because of the higher surface area/volume ratio of the equipments (Kemp, 2017), accounting for the differences in SY. Indeed, thermal efficiencies up to 20.21% were informed by Bordón et al. (2021b), while significantly higher values were calculated in the present study (section 3.2.2).

3.2.2 Thermal efficiency

Thermal efficiencies in dryers are affected by the process conditions, mainly the inlet and outlet drying-air temperatures, and the properties of the feed, for instance, the solid content (Al-Khattawi et al., 2018; Bhandari et al., 2008). As the solids' concentration increases, the heat input necessary for the evaporation of the solvent decreases, thereby rising the thermal efficiency (Anandharamakrishnan & Ishwarya, 2019). The same effect on the thermal efficiency is caused by an increment in the difference $T_{inlet} - T_{outlet}$, that is, by increasing T_{inlet} and operating the dryer at a T_{outlet} as low as the process allows (Masters, 1979); these relationships can be appreciated in Table 3 and Fig. 1. The operation under these conditions involves a lower heat requirement to obtain a unit weight of product, with a constant residual moisture content from a constant solids feedstock (Masters, 1979). Nonetheless, drying processes at such extreme temperatures may damage the oil quality or yield powders with a higher residual moisture content (Bhandari et al., 2008; Masters, 1979).

3.2.3 Estimation of a single droplet evaporation time and additional exposure time of dry microcapsules in the chamber

The atomization of the feed has an important role in dictating the drying kinetics, because it determines the exposed surface area through which heat and mass transfer occur (Bordón et al., 2021b; Lisboa et al., 2018). It is important to point out that the t_{dr} values were based on many simplifications presented in section 2.3.4.3.1. Therefore, they represent theoretical values useful for calculating the dimensions of dryers (Martínez, 2009). Previously, a droplet evaporation time was estimated from the mean or the median of the size distribution of the sprays (Bordón et al., 2021a,b; Lisboa et al., 2018). However, in the present analysis the calculations were based on a more conservative assumption, considering the diameter below which 95 % of the size distribution of the spray lies ($D_{95,1}$); if a droplet with such diameter is dried, then 95 % of the atomized spray will be dried as well (Martínez,2009).

The estimated values of the Sauter mean diameter and of $D_{95,1}$ can be found in **Table 4** and fell within the size distribution normally observed for rotary atomizers (Anandharamakrishnan & Ishwarya, 2015). The calculated values for the total evaporation time t_{dr}, the evaporation times for the constant (t_{cr}) and falling rate (t_{fr}) periods, as well as the regression coefficients of the adjusted models, are listed in Table 3. Moreover, the response surfaces are depicted in Fig. 1. As can be seen from Table 3, there are significant effects ($p \leq 0.05$) of both T_{inlet} and T_{outlet} on t_{dr}, t_{cr} and t_{fr}. Particularly, as T_{outlet} increases, so does the heat transfer to a droplet and t_{dr} decreases (Fig. 1) (Lisboa et al., 2018). The same effect could be appreciated on t_{cr} and t_{fr}. For a given $T_{outlet,}$ higher t_{dr} values were calculated as T_{inlet} increases, which is possibly associated to larger droplet diameters due to risen feed rates(Eq. 6) (Kurozawa et al., 2009). Indeed, Eqs. 5 and 22 show how the length of both drying periods is extended with the increase in the droplet diameter.

In the present analysis, t_{cr} values were higher than t_{fr} (Table 3), as the constant rate period is the time during which the bulk of the evaporation takes place according to Masters (1979). Moreover, the orders of magnitude of the estimated t_{dr} were similar to those informed by Huang et al. (2005), who simulated with a commercial CFD code the drying history of milk suspension droplets produced by a rotary atomizer. For instance, the calculated droplet evaporation time reported by the authors was shorter than 0.80 s, for an atomized droplet whose initial D[3,2] (49.3 μm) was similar to those found in Table 4.

The estimated critical diameters (D_C), which mark the beginning of the falling rate period, can be found in Table 4. Based on Martínez (2009),theD_C values were calculated assuming no droplet collisions, considering negligible changes in the droplet/particle diameter from the critical point to the exit, and that the remaining moisture that was not evaporated until the critical point travels slowly through the capillaries of the solid. Huang et al. (2005) observed a similar evolution of the droplet/particle diameter by simulating the drying history of droplets with initial D[3,2] ranging from 19.1 to 78.1 μm. Curiously, the findings of the present research seem to be in line with Martínez (2009) and Huang et al. (2005)regarding the constant diameter of the droplet/particle from the critical point to the exit. As can be seen in Table 4, the estimated D_C values were underestimated compared with the experimental $D_{95,2}$ observed in dry microcapsules for all the process conditions; nonetheless, the relative deviations between D_C and $D_{95,2}$ were acceptable in all the cases (below 10%).

The additional exposure time of particles (t_{EXP}), once they are in dry-state, may have a remarkable impact on powder quality. Indeed, Bordón et al. (2021b) found significant correlations between t_{EXP} and some properties, such as color (whiteness and yellowness index) and the oxidative status (peroxide index and oxidative stability index) of the powders obtained with two different spray dryers. Regarding the chemical quality of microencapsulated oils, the estimation of t_{EXP} is of paramount importance because once the drying of a droplet is finished, the particle temperature rises until it reaches the outlet of the dryer. The longer this exposure time, the more energy available for deterioration reactions (Bordón et al., 2021b; Schmitz-Schug, 2014).

The calculated values of t_{EXP} were based on the minimum residence time of a particle in the chamber ($t_{res,\,p}$), which was assumed to be equal to the average residence time of air ($t_{res,\,a}$) (Masters, 1979). This last assumption is a simplified approach, given that most of the particles have a residence time much higher than $t_{res,\,a}$: they may be entrapped in recirculating air-flow zones, they may adhere to the chamber walls, or they may travel at lower velocities than the average air velocity (Masters, 1979). Moreover, one point should be clarified: wet droplets of different size are usually found in the same spray, which undergo different drying histories and residence times (Huang et al., 2005). Nonetheless,

this situation was not considered in the simplifications of the present analysis, which focuses on single droplets of the same initial diameter ($D_{95,1}$) whose residence time was assumed to be $t_{res,\,a}$.

The average air residence time for the Niro Production Minor was calculated according to Schmitz-Schug (2014), who modeled the spray-drying process of different model dairy formulations in the same dryer. The author considered plug-flow conditions, therefore $t_{res,\,a}$ was calculated by dividing the chamber volume by the total air flow rate (air volume evaluated at the outlet temperature and relative humidity). For all the process conditions in our study, $t_{res,\,a}$ was around 11 s, which was in accordance with the reported values by Schmitz-Schug et al. (2013)and Schmitz-Schug (2014). Moreover, the $t_{res,\,a}$ values found in the present analysis, for the spray-drying of the same emulsion formulation, were above those of the laboratory-scale dryer Büchi- B290 (around 1.08-1.24 s) and below those of the Niro Mobile Minor (around 15-25 s) (Bordón et al., 2021b). This may be attributed to different chambers' dimensions, the air disperser designs and the relative location between this disperser and the atomizer, which dictate the air trajectory (Masters, 1979).

Once $t_{res,\,a}$ was estimated, t_{EXP} was calculated as $t_{res,\,p} - t_{dr}$. These values, and the regression coefficients of the models fitted as function of T_{inlet} and T_{outlet}, can be found in Table 3. The statistical models fitted for this variable will be useful for the multiple response optimization study (section 3.3), and as observed for t_{dr}, a linear function of T_{inlet} and T_{outlet} could fit the estimated values with a high determination coefficient (R^2). This was expected, given that t_{EXP} was calculated as a difference between a variable that took on discrete values ($t_{res,\,p}$), and the evaporation time that was linearly-dependent on T_{inlet} and T_{outlet}. Once more, it is important to highlight that the estimated values represent a minimum exposure time, because most of the particles show a residence time much higher than the average air residence time. This was demonstrated by Schmitz-Schug (2014), who determined a distribution of particles' residence time experimentally by using fluorescent markers; the median of the distributions were 6 and 17 s for the Büchi- B290 and the Niro Production Minor, respectively.

3.2.4 Physicochemical properties of chia oil microcapsules

The regression coefficients and observed values for the physicochemical properties of microcapsules are shown in Table 5. The first two interrelated properties analyzed are the water activity at 25 °C (a_W) and the moisture content (*MC*). As can be seen from Table 5, these properties fell within the ranges usually observed in food powders (Bhandari & Adhikari, 2008). For the same emulsion formulation, the a_W values were similar to those observed in the Büchi- B290 by Bordón et al. (2021b). In addition, the *MC* of powders in the pilot-scale dryer were similar to the laboratory scale, or even lower for some process conditions (especially at a T_{outlet} = 90 °C). This latter may be attributed to many factors, such as the larger dimensions of the chamber, the higher residence time of particles, and the different air-to-liquid (ALR_{dryer}) ratios of the dryers (Schmitz-Schug et al., 2013). The ALR_{dryer} is obtained by dividing the mass flow rate of the drying-air by the mass flow rate of the solvent in the feed. Therefore, by using the ALR_{dryer} the comparison of spray-drying processes at different scales is possible, despite the differences in geometry and air-flow patterns (Schmitz-Schug et al., 2013). The ALR_{dryer} values were between 116.40-249.94 and 40.46-140.26 for the laboratory and pilot-scale dryers, respectively. As can be appreciated, higher ALR_{dryer}, i.e. higher drying-air mass flow rates were needed in the laboratory scale than in the pilot-scale to obtain a similar drying result, which was also reported for the same spray dryers by Schmitz-Schug (2014). Moreover, the *MC* values found in Table 5 are similar to those informed recently for chia oil microencapsulation by Santos Fernandes et al. (2021) and Copado et al. (2021), who reported values below 3.60%.

The D[4,3] mean diameter of powders was determined (Table 5). Moreover, additional size distribution-related parameters, such as the D[3,2] mean diameter and the polydispersity index (PDI) are given in **Table B1.1** of the supplementary material. In this research, the D[4,3] values for all the process conditions were lower than those of the Niro Mobile Minor, but higher than those observed in the Büchi- B290 according to Bordón et al. (2021b). This might be due to differences in the atomization devices, as well as in the atomization conditions. First, a more efficient droplet fission might be achieved with higher centrifugal accelerations and a larger wheel diameter (Munoz-Iibanez et al., 2015) in the Niro Production Minor, thereby obtaining lower D[4,3] values in final powders compared with the Niro Mobile Minor. Second, the twin fluid nozzle of the Büchi-B290 generally produces smaller droplets than a rotary atomizer, and narrower size distributions reflected by the PDI (Toro-Sierra et al., 2013). Other researchers informed smaller particle sizes for chia oil microcapsules than those in the present study. Nonetheless, nozzle-type atomizers were used: between 12-16 µm (Alcântara et al., 2019) and below 5 µm (Copado et al., 2021; Lavanya et al., 2019; Santos Fernandes et al., 2021)

A normalized value of the median diameter (d_{50}*) was calculated for the reconstituted emulsions after atomization. From **Eq. 25**, it can be observed that a d_{50}*value close to one would indicate non-considerable changes in the size distribution of oil droplets, compared with parent emulsions, after the atomization processes. Therefore, the atomization conditions must be carefully selected for encapsulation purposes based on emulsions (Dubey et al., 2016), given that the size of the dispersed oil droplets in the resulting powder affects the encapsulation efficiency, the physical stability of the final product and the sensory properties of the reconstituted food (Taboada et al., 2021). The d_{50}*values calculated are listed in Table 5 and the size distributions of oil droplets in parent and reconstituted emulsions are depicted in **Fig. 2**. A trend similar to that of the powder particle was observed for the d_{50}*values of reconstituted emulsions, possibly as a consequence of different atomization devices and conditions discussed in the previous paragraph: Büchi- B290 (between 0.70 – 0.94) (Bordón et al., 2021b) < Niro Production Minor (between 1.35-1.66) (Table 5) < Niro Mobile Minor (between 3.96 – 5.29) (Bordón et al., 2021b). Comparing the last two dryers equipped with rotary atomizers, the highest d_{50}*values for the Niro Mobile Minor might be attributed to the poor atomization conditions, as reflected by the differences in the non-dimensional quantity V_{th}* discussed insection 3.1.
Moreover, the significant reduction ($p \leq 0.05$) of the PDI in parent emulsions (2.49±0.01) after atomization (1.10 – 1.60 in reconstituted emulsions, depending on the spray-drying condition), evidences efficient atomization forces (Munoz-Ibanez et al., 2015; Taboada et al., 2021).

The color of food powders was determined, given that it dictates the macroscopic aspect and the sensory properties of the products in which powders are incorporated as ingredients (Bordón et al., 2021b; Copado et al., 2021; González et al., 2016). Regarding microencapsulated oils, whitish particles are usually preferred by manufacturers and consumers over others with a yellowish aspect, because a yellow color can evidence the oxidation of triacylglycerols and free fatty acids (Rodríguez et al., 2019). In this study, whitish powders were obtained with lightness values L* above 90.00 (data not shown). The color was reported as a whiteness index *WI*, which was calculated from the CIELAB coordinates. Similarly, Copado et al. (2021) informed high lightness values for chia oil microcapsules and attributed them to the presence of maltodextrin in the wall material. According to Table 5, the *WI* values of this research were slightly below those recorded for the Büchi- B290, but above those of the Niro Mobile Minor (Bordón et al., 2021b). These results might be due to differences in the residence time of the particles and in the oxidative status of microencapsulated oils. Indeed, Bordón et al. (2021b) found that *WI* and t_{EXP}, as well as the oxidative stability index (OSI)and t_{EXP}, were

significantly and negatively correlated, evidencing that the color of powders obtained in different spray dryers may be associated to the extent of oxidation reactions occurring in microencapsulated oils.

A significant problem associated with microencapsulated oils is their poor flowability (Drusch et al., 2006). This flow is governed by different physical properties of powders, such as the particle size distribution and shape, moisture content and time-consolidation (Rodríguez et al., 2019). Moreover, different roles were attributed to the moisture content, the non-encapsulated oil fraction and electrostatic interactions, on the cohesive forces that arise between particles (Drusch et al., 2006; Emery et al., 2009; Schmitz-Schug, 2014). The flowability of powders was assessed through the Carr's Index (CI) and the Hausner ratio (HR), which can be found in Table 5. According to these values, the products are below the limit of a free-flowing and non-free flowing powder (~ 25%). In addition, given that all the HR were below 1.25, the powders can be classified as easy-to-fluidize (Rodríguez et al., 2019). It is worth pointing out that the products obtained with the Niro Production Minor exhibited a better flowability than those from the Büchi-B290 and the Niro Mobile Minor. For these latter dryers, the CI and HR were between 31.48-49.67 and 1.46-1.95, respectively (data not published by our research group). The differences in the flow properties may be due to different factors. First, as particle size decreases, the cohesive forces become predominant and the flowability is worsen (Emery et al., 2009), which would explain the results for the powders produced by the twin fluid nozzle atomizer in Büchi-B290. Recently, Copado et al. (2021) informed CI values between 36-44% for chia oil microcapsules produced in the same laboratory-scale dryer, and these values were mainly attributed to the small particle sizes. Second, significantly higher ($p \leq 0.05$) *MC* values were found (5.07-6.54 %, wet basis) by Bordón et al. (2021b) for products obtained with the Niro Mobile Minor. Among other factors, the powders' moisture content may be considered as inversely correlated to their capacity to flow (Juarez-Enriquez et al., 2017). Third, the more spherical shape and the higher bulk density of the products obtained at pilot plant, compared with smaller-scale dryers, have also be considered by other authors (Al-Khattawi et al., 2018; Kurozawa et al., 2009; Poozesh & Bilgili, 2019). Indeed, some studies point out that powders containing spherical particles show good flowability as compared with those with elongated or irregular shape, because these latter might tend to mechanically interlock or entangle with each other, thus obstructing powder flow and reducing flowability (Kurozawa et al., 2009). The spherical shape of the products obtained in the present research will be further discussed in section 3.5.2.

The encapsulation efficiencies observed with different process conditions can be found in Table 5. These values were above 90% and were similar to those informed previously by other authors for the microencapsulation of chia oil (Copado et al., 2019, 2021; Julio et al., 2019; Us-Medina et al., 2018). Moreover, it is worth highlighting that the *EE* values were higher than those reported by Bordón et al. (2021b) for products obtained with the Büchi- B290 (61.51-74.53%). This might be attributed to the smaller particle size achieved with the twin fluid nozzles, compared with rotary atomizers, because the smaller the particle size, the less surface is exposed and less surface oil is extracted (Anandharamakrishnan & Ishwarya, 2015).

As regards the bioaccessible oil after an *in-vitro* digestion process, it has been reported previously by many authors that the non-lipid components of a delivery system (proteins, polysaccharides or fibres) affect the degree of lipid digestion (Timilsena et al., 2017). Other physicochemical properties of powders, such as their particle size, interfacial characteristics and the degree of crystallization of the lipid compounds, have also been reported by different authors as influencing factors on the degree of digestion (Augustin et al., 2014). Given the presence of non-lipid components in the microcapsules, the bioaccessible oil after ingestion and passage through the gastrointestinal tract was quantified

(Bordón et al., 2021b; González et al., 2018). The results observed from Table 5 indicate that a high amount of the oil originally incorporated in the formulation was released from the matrix. Similar results were informed by Bordón et al. (2021b)for the same emulsion formulation processed in two different spray dryers (between 94 – 96 % of the oil was released), by González et al. (2018)and Gañán et al. (2020)for chia oil microencapsulated in soy protein isolate microparticles by freeze-drying (94.83±2.57 %) and CO_2-assisted impregnation (95.69±4.28 %), respectively. In addition, Timilsena et al. (2017) reported a high oil release (>95%) for chia oil encapsulated in a different complex coacervate system than ours, formulated with chia mucilage and chia protein isolate.

Finally, the oxidative stability index (OSI) of microencapsulated oils was determined and expressed as an induction time (*IT*) in hours. First, it should be clarified that the *IT* for the unencapsulated chia oil was 3.57±0.15 h. As can be observed from Table 5, all the *IT* recorded for microencapsulated oils were significantly higher ($p \leq 0.05$) than that of pure chia oil. The values were similar to those informed previously for microencapsulated chia oil obtained in the Büchi- B290, and higher than the *IT* values recorded for products from the Niro Mobile Minor (Bordón et al., 2021b). These results indicate that the microencapsulation process by complex coacervation and subsequent spray-drying effectively protects the chemical quality of chia oil. Moreover, not only higher solid yields and thermal efficiencies were achieved after the scale-up of the spray-drying operation, but also the oxidative stability of the core material was preserved despite the longer residence times of particles in a chamber of larger dimensions, compared with the Büchi-B290 (Bordón et al., 2021b). Previously, Us-Medina et al. (2018) informed similar (5.01-6.51 h) *IT* values with sodium caseinate+lactose or sodium caseinate+lactose+chia mucilage, and higher (7.51-13.90 h) values in the absence of lactose and inclusion of maltodextrin or chia seed protein fraction in the wall material formulation. The authors explained that the oxidative stability was not necessarily correlated to the encapsulation efficiency, but to the molecular weight and barrier properties of the wall material.

3.3 Spray-drying experimental design: Multiple response optimization

A multiple response optimization study was performed within the explored experimental domain, in a similar manner as done previously for the Niro Mobile Minor (Bordón et al., 2021a)and the Büchi- B290 (Bordón et al., 2021b) spray dryers. The optimization study was based on the regression models (Tables 3 and 4) and on the optimization goals (**Table 6**). Some of these goals are clear, while others were justified by Bordón et al. (2021a,b).Two more goals should be clarified. First, the particle size given by the D[4,3] mean diameter should be minimized. However, as the particle size decreases, the cohesion forces entail challenges in container filling and problems with the flowing of the powder (Rodríguez et al., 2019). Given that chia oil microcapsules are designed as an omega-3-rich ingredient, whose final destination is to be incorporated in a specific food matrix, these powders must not modify the external appearance of the food product (González et al., 2016). Therefore, the mean particle size should be minimized, but at the same time the powder flowability should be maximized, i.e., by minimizing the Carr's Index (CI) and the Hausner ratio (HR). Second, between the droplet evaporation time, t_{dr}, and the additional exposure time, t_{EXP}, this latter was selected because it represents the largest part of the average particle residence time, as can be appreciated from the comparison between t_{dr} andt_{EXP}(Table 3).

The processing condition that simultaneously optimized all the dependent variables within the explored experimental domain was 160 °C x 90 °C (T_{inlet} x T_{outlet}), with the maximum predicted overall desirability: D_0 = 0.73. This results were in agreement to the optimum drying conditions established previously (Bordón et al., 2021b) for the laboratory-

scale dryer Büchi-B290: 160 °C x 2.8 mL/min (T_{inlet} x V_{feed}), for which the corresponding experimental T_{outlet} was 91.5±2.12 °C. Hence, the optimum process conditions for the same emulsion formulation were similar across scales.

With the aim of validating the regression models and the predicted optimum, three independent drying experiments were performed under these optimum conditions. The relative deviation between the experimental and predicted responses can be found in Table 6. The *AAD*, A_f and B_f, (Eqs. (2a)–(2c)) were calculated, except for the additional exposure time t_{EXP}, which was a theoretical variable that could not be validated directly. The regression models allowed a high prediction level for the dependent variables chosen.

3.4 Spray-drying experimental design: Additional characterization of microcapsules obtained under the optimum processing conditions

After establishing the optimum process conditions at pilot-scale, the physicochemical stability of chia oil within the microcapsules' structure was further analyzed. Therefore, the fatty acid composition of microencapsulated oils before and after *in-vitro* digestion and the thermal stability under air-flow conditions.

The fatty acid composition (relative abundance) for bulk and microencapsulated oils (before and after *in-vitro* digestion) is depicted in the supplementary **Fig. B2.1**. It is of paramount importance that the α-Linolenic acid content of bulk chia oil is preserved through the subsequent processing steps. No significant differences ($p>0.05$) were found among samples compared with bulk oil (66.00±0.21 %). Indeed, neither the microencapsulation process by spray-drying (64.53±0.07 %) nor the *in-vitro* digestion (59.09±3.24 %) affected significantly the α-Linolenic acid content. These results are in line with those discussed in section 3.2.4, regarding the preservation of the oxidative stability of chia oil even after scale-up of the spray-drying operation.

The thermal stability of the optimal product was assessed under a non-inert atmosphere by DSC techniques, which are a good alternative to determine kinetic parameters for oxidation reactions of lipids (Guimarães-Inácio et al., 2018). Previously, several authors explained that the DSC oxidation curves usually exhibit similar features, which can be associated to the chain reaction scheme of lipid oxidation (Litwinienko & Kasprzycka-Guttman, 1998). As a first step (the initiation stage), the heat flow signal separates from the baseline. The sudden increase in the signal and the first peak are attributed to the propagation step and to the formation of non-radical stable products (termination step), respectively. Moreover, a second peak may be observed, which has been associated to hydroperoxide decomposition (secondary oxidation mechanisms) (Guiotto et al., 2014).

The DSC curves of bulk and microencapsulated oils at different heating rates are shown in the supplementary **Fig. B2.2**. In addition, the onset temperature for each heating rate (T_{onset}), the activation energy (E_a) calculated with the method of Ozawa, Flynn and Wall (OFW) (Eqs. 31-32) (Flynn & Wall, 1966; Ozawa, 1970) and the determination coefficients for the OFW method are given in **Table 7**. As can be observed in Fig. B2.2 and in Table 7, T_{onset} shifted significantly ($p\leq0.05$) towards higher values after microencapsulation, supporting the protective effect of the wall material by delaying the onset of oxidation reactions (Guimarães-Inácio et al., 2018). Second, it should be pointed out that bulk chia oil obtained in this research by solid-liquid extraction showed a similar E_a to that of chia oil extracted by screw-pressing (71.83±5.72 kJ/mol) (Bordón et al., 2021b). Moreover, in our previous study, the microencapsulation process at laboratory scale in the Büchi- B290 effectively increased the E_a (95.57±1.94 kJ/mol), which is the energy barrier that

should be overcome for the propagation of oxidation reactions. Similarly, in the present analysis, the microencapsulation process at pilot-scale in the Niro Production Minor increased significantly (97.00±4.29 kJ/mol), compared with bulk chia oil. These results are in line with the induction times discussed before (section 3.2.4) and, once more, indicate that the scale-up of the spray-drying operation did not alter significantly the chemical quality of the microencapsulated oil. Guimarães-Inácio et al. (2018) reported a similar E_a (97.3±2.9 kJ/mol) for chia oil microencapsulated in a carnauba wax matrix by freeze-drying. It is worth highlighting that the authors obtained this value working with DSC techniques under air-flow conditions (not with pure oxygen) and with a 2/1 wall/core ratio (w/w), in a similar manner as in our study. This latter information is important for a valid comparison of results.

3.5 Comparison between chia oil microcapsules and blank microparticles

As explained above, blank dispersions (devoid of chia oil) were also spray dried, exactly as performed with the O/W emulsions. The aim was to analyze how specific properties of powders are affected by the incorporation of the core material. Some of these properties for blank microparticles are listed in **Table 8**. The first outstanding feature is the significantly higher ($p \leq 0.05$) *MC* for blank microparticles than for microcapsules. However, no significant differences ($p > 0.05$) were observed in a_W for both types of powders. A plausible reason for the higher *MC* in the absence of oil may be related to the different moisture sorption behavior. Indeed, our research group recorded a higher monolayer content W_m for blank microparticles (5.207±0.128g water/100 g dry solids) than for microcapsules (3.721±0.136 g water/100 g dry solids) obtained at laboratory-scale (Bordón et al., 2021c). These results indicate more available sorption sites or an enhanced water-holding capacity of powders in the absence of oil (Murrieta-Pazos et al., 2011). The redispersion of powders is another property affected by the availability of active sorption sites (section 3.4).

Regarding the size distribution of powders, Table 8 shows significantly lower ($p \leq 0.05$) values for the D[4,3] mean diameters in blank microparticles. Similarly, lower D[3,2] values can be found in Table B1.1 for the absence of oil. These results are expected, since oil droplets disturb the fluid flow and promote a higher energy dissipation. Therefore, the atomization forces are more efficient in the absence of oil, and the final particle size decreases (Kurozawa et al., 2009).

The color of powders was also affected by the presence of chia oil. For all the spray-drying conditions, the *WI* was significantly higher ($p \leq 0.05$) for the blank microparticles than for chia oil microcapsules. Gañán et al. (2020)informed similar results for soy protein microparticles after the supercritical CO_2-assisted impregnation of chia oil, which is expected given the original color of the oil.

Another outstanding difference between both types of powders was detected in their flowing behavior. Significantly lower ($p \leq 0.05$) compressibility values or CI were recorded for blank microparticles than for microcapsules. The HR followed the same trend (Table 8). As can be seen, the higher compressibility after the incorporation of the core material evidences a more cohesive powder (Rodríguez et al., 2019). As discussed above (section 3.2.4), several factors can influence the flow properties. Among them, the non-encapsulated oil fraction may play a key role in the present analysis, turning the surface of particles more cohesive (Murrieta-Pazos et al., 2011)and limiting the flowability (Drusch et al., 2006).

3.5.1 Back scattering profile after redispersion

The ease of redispersion of powders limits its potential applications in different food matrices, especially in the case of

oil microcapsules, since the stable behavior of the original emulsion should be reproduced (Copado et al., 2019, 2021; Ixtaina et al., 2015). In order to study the physical stability of the redispersed systems, the light backscattering profile was followed in a vertical analyzer during 48 h (**Fig. 3**). As can be observed, noticeable changes were found at the bottom of the tubes corresponding to microcapsules, except for one drying condition (160 °C x 90 °C, T_{inlet} x T_{outlet}). More precisely, a rise in %backscattering was observed as time elapsed, which is possibly attributed to the increase in the content of sedimented particles. On the contrary, no significant changes were recorded in the %backscattering for blank microparticles, in the same area of the tube.

The electrical charge of particles is a well-known mechanism that allows to keep them suspended, due to the repulsive forces that arise between them (Julio et al., 2018). However, both oil microcapsules and blank microparticles show almost null electrical charge due to complex coacervation. As can be seen, the electrical charge is not sufficient to explain the different redispersion behavior. Among diverse factors, the availability of active sites for moisture sorption (section 3.4) may account in part for the observed results. Indeed, the presence of polar residues on the surface has a key role in the sequence of phenomena that take place during the reconstitution of powders (Fang et al., 2008).

Finally, although the general trend regarding the redispersion of microcapsules evidences an increase in %backscattering at the bottom of the tubes, the powders obtained under the optimum spray-drying conditions were the exception. According to Table B1.1, these microcapsules exhibited the smallest particle size ($p \leq 0.05$) given by the D[3,2] mean diameter. Consequently, their specific surface area is the highest, as well as their affinity for moisture (Kurozawa et al., 2009). In addition, it has been experimentally shown in the case of sparingly soluble materials, that the speed of redispersion increases with decreasing particle size (Buckton & Beezer, 1992).

3.5.2 Morphology

The morphology of powders was assessed by SEM micrographs (**Figs. 4** and **5**). First, it should be highlighted, for all the spray-drying conditions (Fig. 4), the presence of spherical particles usually produced by rotary atomizers (O' Sullivan et al., 2019). Similarly, other authors have previously reported on the presence of more spherical particles after scale-up of the spray-drying operation, compared with the laboratory-scale (Poozesh & Bilgili, 2019; Al-Khattawi et al., 2018).

The surface of particles exhibited a rough appearance with some depressions. In some cases, especially in the absence of oil, particles with a smooth surface were also observed. A rough appearance and shallow depressions are usual during spray-drying (Anandharamakrishnan & Ishwarya, 2015)and have been attributed to the interaction among diverse factors: atomization mechanisms, evaporation rate, a possible uneven shrinkage during the constant rate period and the viscoelastic properties of the wall materials (Anandharamakrishnan & Ishwarya, 2019). Moreover, in some images red arrows can be found pointing to few blow-holes. The presence of these holes (only a few were found) is mainly due to the permeable nature of the droplet/particle during drying, which allows the flow of water vapor and dissolved gases from the inside to the surface. When large droplets are dried at a temperature above that of the evaporation of water, these can swell after the formation of the solid layer due to the increased internal pressure. This phenomenon can cause a rupture of the outer wall, giving rise to the holes (Walton & Mumford, 1999). The presence of the few holes found allowed to appreciate a hollow internal structure (Fig. 5), both in microcapsules and blank microparticles. Indeed, hollow particles are usually obtained from materials with a skin-forming capacity (Walton & Mumford, 1999). A final interesting feature to point out is the internal microstructure of powders. The microcapsules

clearly exhibited a matrix-type structure, as can be deduced from the small gaps in the internal face (Fig. 5 A and B). Certain authors have discussed that the oil droplets are located in these small gaps (Copado et al., 2019; Taboada et al., 2021), which notably were not observed in blank microparticles (Fig. 5 C and D).

4 Conclusion

The drying-air inlet (T_{inlet}) and outlet temperatures (T_{outlet}) were studied as experimental factors for the microencapsulation of chia oil by spray-drying at pilot-scale. After scale-up of the spray-drying operation, significantly higher solid yields (74.24-79.79 %) and thermal efficiencies (27.56-73.19 %) were recorded, compared with previous experiments at laboratory scale. It is worth pointing out that whitish products were obtained, with enhanced encapsulation efficiencies and flowability compared with powders from the laboratory-scale. In addition, the process scale-up did not affect the following properties: the amount of bioaccessible oil after *in-vitro* digestion processes; the fatty acid composition of microencapsulated oils before and after *in-vitro* digestion; the chemical quality of microencapsulated oils as reflected by the induction times and the oxidation kinetic parameters elucidated from DSC. A multiple response optimization analysis was performed at pilot-scale. The process conditions that simultaneously optimized all the responses were 160 °C x 90 °C (T_{inlet} x T_{outlet}). Similarly, the optimum process conditions established previously for the laboratory-scale was 160 °C x 2.8 mL/min (T_{inlet} x V_{feed}), for which the experimental T_{outlet} was 91.5±2.12 °C. Therefore, the optimum process conditions for the same emulsion formulation were similar across the analyzed scales.

As a concluding remark, the main goal for the scale-up of the spray-drying unit operation from the laboratory to pilot-scale was fulfilled in the present research, not only by increasing the solid yield and thermal efficiency, but also through the preservation of important physicochemical properties and the microstructure of chia oil microcapsules. Moreover, the enhanced understanding of the spray-drying process achieved through the optimization at pilot-scale, and the simple phenomenological model used to estimate droplet drying times are intended to set the basis for future functional powders' application and development at industrial-scale.

Declaration of competing interest

The authors declare no conflict of interest.

Declaration of interests

☒The authors declare that they have no known competing financial interests or personal relationships that could have appeared to influence the work reported in this paper.

Data availability statement

The data sets generated during and/or analyzed during the current study are available from the corresponding author on reasonable request.

Acknowledgements

This research was financed with grants from Consejo de Investigaciones Científicas y Técnicas (CONICET), Argentina. The authors would like to acknowledge the Iberoamerican Project CYTED 119RT0567. María Gabriela Bordón would like to acknowledge the fellowships from CONICET and from Secretaría General Iberoamericana-Fundación Carolina.

Appendix A. Related information for modeling

A.1. Enthalpy of vaporization (J/kg).

$$\Delta H_{vap} = 2.792x10^6 - 160T - 3.43T^2 \text{(Langrish, 2009)} \quad \textbf{(A1)}$$

In the above equation, T corresponds to the wet-bulb temperature (T_{wb}) in K.

A.2. Specific heat capacities.

A.2.1. Drying air

$$Cp_{drying\ air} = 1.005 + 1.880\ Y \quad \textbf{(A2)}$$

where 1.005 and 1.880 kJ/kg.K are the specific heat capacities of dry air ($Cp_{dry\ air}$) and vapor (Cp_{vapor}), respectively (Langrish, 2009); Y is the absolute humidity (kg water/kg dry air).

A.2.2. Feed

$$Cp_{feed} = (Cp_{dry\ solid} + Cp_{water}\ W_1).(1\text{-}W_{1,\ w.b}) \quad \text{(Treybal, 1980)} \quad \textbf{(A3)}$$

$$Cp_{dry\ solid} = Cp_{carbihydrate}x'_{carbohydrate} + Cp_{protein}x'_{protein} + Cp_{lipid}x'_{lipid} + Cp_{ash}x'_{ash}$$

(J/kg.K) (Shamaei et al., 2017) **(A4)**

where $x'$is a mass fraction calculated on a dry basis (-). Expressions for the Cp for each component can be found in Shamaei et al. (2017).

A.3. Thermal conductivity of the air film surrounding a droplet.

$$k_d = 1.5207 \times 10^{-11} T_{film}{}^3 - 4.8574 \times 10^{-8} T_{film}{}^2 + 1.0184 \times 10^{-4} T_{film} - 0.000393$$ (Patel et al., 2010)

(mW/m.K) **(A5)**

where k_d should be calculated at the mean film temperature surrounding a droplet (T_{film}), which can be conveniently taken as the average between T_{outlet} and the droplet surface temperature. This latter is the adiabatic saturation temperature (Masters, 1979).

References

Alcântara, M.A., Alcântara de Lima, A.E., Mattos Braga, A.L., Valeriano Tonon, R., Galdeano, M.C., da Costa Mattos, M., et al. 2019. Influence of the emulsion homogenization method on the stability of chia oil microencapsulated by spray drying. Powder Technol., 334, 1-8.

Al-Khattawi, A., Bayly, A., Phillips, A., Wilson, D.2018. The design and scale-up of spray dried particle delivery systems. Expert Opin. Drug Deliv., 15,47–63.

Amaya Cano, J.S., Segura Pacheco, S., Salcedo Galán, F., Arenas Bustos, I., Rincón Durán, C., Hernández Carrión, M. 2021. Formulation of a responsive *in vitro* digestion wall material, sensory and market analyses for chia seed oil capsules. J. Food Eng., 296, 110460.

Anandharamakrishnan, C., Ishwarya, S.2015. Spray Drying Techniques for Food Ingredient Encapsulation, John Wiley & Sons Ltd, UK.

Anandharamakrishnan, C., Ishwarya, S.2019. Essentials and Applications of Food Engineering, CRC Press, Taylor & Francis Group, Boca Raton, FL, USA,pp. 363-375.

Augustin, M. A., Sanguansri, L., Rusli, J. K., Shen, Z., Cheng, L. J., Keogh, J., et al. 2014. Digestion of microencapsulated oil powders: In vitro lipolysis and in vivo absorption from a food matrix. Food Funct. (11), 2905-2912.

Bhandari B.R., Adhikari, B.P. 2008. Water activity in food processing and preservation, In: X.D. Chen, A.S. Mujumdar (eds.). Drying Technologies in Food Processing,John Wiley & Sons Ltd., West Sussex, UK, pp. 55-86.

Bhandari, B.R., Patel, K.C., Chen, X.D.2008. Spray drying of food materials- process and product characteristics, In: X.D. Chen, A.S. Mujumdar (eds.), Drying Technologies in Food Processing. West Sussex, UK, John Wiley & Sons Ltd., pp. 113-157.

Bodoira, R.M., Penci, M., Ribotta, P., Martínez, M. 2017. Chia (Salvia hispanical.) oil stability: Study of the effect of natural antioxidants. LWT-Food Sci.Technol., 75, 107–113.

Bordón, M.G., Alasino, N.P.X., Camacho, N., Yonaha, V., Defain Tesoriero, M.V., Ribotta, P.D., Martínez, M.L. 2021a. Spray-air contact and operating conditions in tall and short-form co-current spray dryers affect relevant physico-chemical properties of microencapsulated chia oil (*Salvia hispanica* L.). Food Bioprod. Process., 127, 309-327.

Bordón, M.G., Alasino, N.P.X., Martínez, V., Gauna Peter, R., Iturralde, R., Ribotta, P.D., Martínez, M.L. 2021b. Influence of the spray drying operating conditions on the estimated drying kinetics of emulsion single droplets and the properties of microencapsulated chia oil. Powder Technol., 383, 302-317.

Bordón, M.G., Paredes, A.J., Camacho, N.M., Penci, M.C., González, A., Palma, S.D., Ribotta, P.D., Martínez, M.L. 2021c. Formulation, spray-drying and physicochemical characterization of functional powders loaded with chia seed oil

and prepared by complex coacervation. Powder Technol., 391, 479-493.

Bordón, M.G., Meriles, S.P., Ribotta, P.D., Martínez, M.L.2019. Enhancement of composition and oxidative stability of chia (Salvia hispanical.) seed oil by blending with specialty oils. J. Food Sci., 84 (5), 1035–1044.

Buckton, G., Beezer, A.E. 1992. The relationship between particle size and solubility. Int. J. Pharm., 82, 7-10.

Charoo, N.A., Shamsher, A.A.A, Zidan, A.S., Rahman, Z. 2012. Quality by design approach for formulation development. A case study of dispersible tablets. Int. J. Pharm., 423, 167-178.

Copado, C.N., Diehl, B.W.K., Ixtaina, V.Y., Tomás. M.C. 2019.Improvement of the oxidative stability of spray-dried microencapsulated chia seed oil using Maillard reaction products (MRPs). Eur. J. Lipid Sci. Technol., 121 (7), 1800516.

Copado, C.N., Julio, L.M., Diehl, B.W.K., Ixtaina, V.Y., Tomás. M.C. 2021. Multilayer microencapsulation of chia seed oil by spray-drying using electrostatic deposition technology. LWT-Food Sci. Technol., *In Press*, 112206 .

Desobgo, Z.S.C., Stafford, R.A., Metcalfe, D.J.A. 2015. Dimethyl sulfide stripping behavior during wort boiling using response surface methodology. J. Am. Soc. Brew. Chem., 1, 84–89.

Di Battista, C.A., Costenla, D., Ramírez-Rigo, V., Piña, J. 2017. Process analysis and global optimization for the microencapsulation of phytosterols by spray drying. Powder Technol., 321, 55-65.

Drusch, S., Serfert, Y., Schwarz, K.2006. Microencapsulation of fish oil with *n*-octenylsuccinate-derivatised starch: Flow properties and oxidative stability. Eur. J. Lipid Sci. Technol., 108, 501-512.

Dubey, B., Case, W., Windhab, E.J. 2016. Processing of functional capsule powder particles based on multiple emulsions using a prilling process. In: U. Fritsching (Ed.), Process-Spray. Functional Particles Produced in Spray Processes, Springer, Switzerland, pp. 941–986.

Emery, E., Oliver, J., Pugsley, T., Sharma, J., Zhou, J. 2009. Flowability of moist pharmaceutical powders. Powder Technol., 189, 409-415.

Escalona-García, L.A., Pedroza-Islas, R., Natividad, R., Rodríguez-Huezo, M.E., Carrillo-Navas, H., Pérez-Alonso, C. 2016. Oxidation kinetics and thermodynamic analysis of chia oil microencapsulated in a whey protein concentrate-polysaccharide matrix. J. Food Eng., 175, 93–103.

Fang, Y., Selomulya, C., Chen, X.D. 2008. On measurement of food powder reconstitution properties. Dry. Technol., 26, 3-14.

Flynn, J.H., Wall, L. A. 1966. A quick, direct method for the determination of activation energy from thermogravimetric data. J. Polym. Sci. B, 4(5), 323–328.

Gañán, N., Bordón, M.G., Ribotta, P.D., González, A.2020. Study of chia oil microencapsulation in soy protein microparticles using supercritical CO_2-assisted impregnation. J. CO_2 Util., 40, 101221.

Gili, R.D., Torrez Irigoyen, M., Penci, M.C., Giner, S.A., Ribotta P.D.2017. Physical characterization and fluidization design parameters of wheat germ. J. Food Eng., 212, 29-37.

González, A., Martínez, M., León, A.E., Ribotta, P.D.2018. Effects on bread and oil quality after functionalization with microencapsulated chia oil. J. Sci. Food Agric., 98 (13), 4903–4910.

González, A., Bordón, M.G., Bustos, M.C., Córdova Salazar, K.L., Ribotta, P.D., Martínez, M.L. 2021. Study of the incorporation of native and microencapsulated chia seed oil on pasta properties. Int. J. Food Sci. Technol., 56 (1), 233-241.

González, A., Martínez, M.L., Paredes, A.J., León, A.E., Ribotta, P.D.2016. Study of the preparation process and variation of the wall components in chia (Salvia hispanica L.) oil microencapsulation. Powder Technol., 301, 868–875

Guimarães-Inácio, A., Lopes Francisco, C.R., Maeda Rojas, V., de Souza Leone, R., Valderrama, P., Bona E., et al. 2018. Evaluation of the oxidative stability of chia oil-loaded microparticles by thermal, spectroscopic and chemometric methods. LWT Food Sci. Technol., 87, 498–506.

Guiotto, E., Ixtaina, V., Nolasco, S., Tomás, M.2014.Effect on storage conditions and antioxidants on the oxidative stability of sunflower-chia oil blends. J. Am. Oil Chem. Soc., 91, 767-776.

Holgado, F., Márquez-Ruiz, G., Ruiz-Méndez, M.V., Velasco, J.2019. Effects of the drying method on the oxidative stability of the free and encapsulated fractions of microencapsulated sunflower oil. Int. J. Food Sci. Technol., 54 (8), 2520-2528.

Huang, L.X., Passos, M.L., Kumar, K., Mujumdar, A.S. 2005. A three-dimensional simulation of a spray dryer fitted with a rotary atomizer. Dry. Technol., 23 (9–11), 1859–1873

Ixtaina, V.Y., Julio, L.M., Wagner, J.R., Nolasco, S.M., Tomás, M.C.2015. Physicochemical characterization and stability of chia oil microencapsulated with sodium caseinate and lactose by spray-drying. Powder Technol., 271, 26–34.

Juarez-Enriquez, E., Olivas, G.I., Zamudio-Flores, P.B., Ortega-Rivas, E., Perez-Vega, S., Sepulveda, D.R.2017. Effect of water content on the flowability of hygroscopic powders. J. Food Eng., 205, 12-17.

Julio, L.M., Copado, C.N., Crespo, R., Diehl, B.W.K., Ixtaina, V.Y., Tomás, M.C.2019.Design of microparticles of chia seed oil by usinf the electrostatic layer-by-layer deposition technique. Powder Technol., 345, 750-757.

Julio, L.M., Copado, C.N., Diehl, B.W.K., Ixtaina, V.Y., Tomás M.C.2018. Chia bilayer emulsions with modified sunflower lecithins and chitosan as delivery systems of omega-3 fatty acids.LWT-Food Sci. Technol., 89, 581–590.

Kemp, I.C., Hartwig, T., Herdman, R., Hamilton, P., Bisten, A., Bermingham, S.2016. Spray drying with a two-fluid

nozzle to produce fine particles: atomization, scale-up and modeling. Dry. Technol., 34 (10), 1243-1252.

Kemp, I.C.2017. Drying of pharmaceuticals in theory and practice. Dry. Technol., 35, 918–924.

Kurozawa, L.E., Gomes Morassi, A., Vanzo, A.A., Park, K.J., Dupas Hubinger, M.2009. Influence of spray drying conditions on physicochemical properties of chicken meat powder. Dry. Technol., 27(11), 1248-1257.

Langrish, T.A.G.2009. Multi-scale mathematical modelling of spray dryers.J. Food Eng., 93, 218–228.

Lavanya, M.N., Kathiravan, T., Moses, J.A., Anandharamakrishnan, C. 2020. Influence of spray-drying conditions on microencapsulation of fish oil and chia oil. Dry. Technol., 38 (3), 279-292.

Lisboa, H.M., Duarte, M.E., Cavalcanti-Mata, M.E.2018. Modeling of food drying processes in industrial spray dryers. Food Bioprod. Process., 107, 49–60.

Litwinienko, G., Kasprzycka-Guttman, T.1998. A DSC study on thermoxidation kinetics of mustard oil. Thermochim. Acta, 319 (1–2), 185–191.

Martínez, L.A. 2009.Dimensionamiento y simulación de un secador por aspersión de nivel piloto. Master Thesis in spanish, Instituto Politécnico Nacional. Unidad Profesional Interdisciplinaria de Biotecnología, Mexico,.

Martínez, M.L., Bordón, M.G., Lallana, R.L., Ribotta, P.D., Maestri, D.M.2017. Optimization of sesame oil extraction by screw-pressing at low temperature. Food Bioprocess Technol., 10 (6), 1113–1121.

Masters, K.1979. Spray drying fundamentals: process stages and layouts, Spray Drying Handbook, 3rd ed. Longman Scientific Technical, Essex, UK.

Munoz-Ibanez, M., Azagoh, C., Dubey, B.N., Dumoulin, E., Turchiuli, C.2015. Changes in oilin-water emulsion size distribution during the atomization step in spray-drying encapsulation. J. Food Eng., 167 (B), 122–132

Murrieta-Pazos, I., Gaiani, C., Galet, L., Cuq, B., Desobry, S., Scher, J.2011. Comparative study of particle structure evolution during water sorption: Skim and whole milk powders. Colloids Surf. B Biointerfaces, 87, 1-10.

Noello, C., Carvalho, A.G.S, Silva, V.M., Hubinger, M.D. 2016. Spray dried microparticles of chia oil using emulsion stabilized by whey protein concentrate and pectin by electrostatic deposition. Food Res. Int., 89, 549-557.

O' Sullivan, J.J., Norwood, E-A., O' Mahony, J.A., Kelly, A.L.2019. Atomisation technologies used in spray drying in the dairy industry: a review. J. Food Eng., 243, 57- 69.

Oliveira, R., Rodríguez, M.F. Bernardo-Gil, M.A. 2002. Characterization and supercritical carbon dioxide extraction of walnut oil. J. Am. Oil Chem. Soc., 79, 225-230.

Ozawa, T. 1970. Kinetic analysis of derivative curves in thermal analysis. J. Therm. Anal. Calorim., 2(3), 301–324.

Patel, K., Chen, X.D., Jeantet, R., Schuck, P.2010. One-dimensional simulation of co-current, dairy spray drying systems- pros and cons. Dairy Sci.Technol., 90, 181-210.

Pharmacopeia. 2000. National formulatory (USP 24 NF 19), MD, U.S: Rockville.

Poozesh, S., Bilgili, E.2019. Scale-up of pharmaceutical spray drying using scale-up rules: a review. Int. J. Pharm., 562, 271–292.

Punia, S., Sandhu, K.S., Siroha, A.K., Dhull, S.B.2019. Omega 3-metabolism, absorption, bioavailability and health benefits–a review. PharmaNutrition, 10, 1–7.

Rodríguez, E.S., Julio, L.M., Henning, C., Diehl, B.W.K., Tomás, M.C., Ixtaina, V.Y.2019. Effect of natural antioxidant on the physicochemical properties and stability of freeze-dried microencapsulated chia seed oil. J. Sci. Food Agric., 99 (4), 1682–1690.

Santos Fernandes, S., Greque, L., Santos, M. de F.C., de Novais, L.M.R., D'Oca, C.D.R.M., Prentice, C., Salas-Mellado, M. de las M. 2021. Effect of the spray drying conditions on the physicochemical and structural characteristics and the stability of chia oil microparticles. J. Appl. Polym. Sci., 135 (39), 51015.

Schmitz-Schug, I. 2014. *Improving the nutritional quality of dairy powders-analyzing and modeling lysine loss during spray drying as influenced by drying kinetics, thermal stress, physical state and molecular mobility*, Lehrstuhl für Lebensmittelverfahrenstechnik und Molkereitechnologie. Verlag Dr. Hut, Munich, Germany,, Doctoral Thesis.

Schmitz-Schug, I., Foerst, P., Kulozik, U.2013. Impact of the spray drying conditions and residence time distribution on lysine loss in spray dried infant formula. Dairy Sci. Technol., 93, 443–462.

Shamaei, S., Seiiedlou, S., Aghbashlo, M., Valizadeh, H.2017. Mathematical modeling of drying behavior of single emulsion droplets containing functional oil. Food Bioprod. Process., 101, 100-109.

Taboada, M.L., Chutani, D., Karbstein, H.P., Gaukel, V.2021. Breakup and coalescence of oil droplets in protein-stabilized emulsions during the atomization and the drying step of a spray drying process. Food Bioprocess Technol., 14, 854-865.

Timilsena, Y.P., Adhikari, R., Barrow, C.J., Adhikari, B. 2016. Microencapsulation of chia seed oil using chia seed protein-chia seed gum complex coacervates. Int. J. Biol. Macromol., 91, 347-357.

Timilsena, Y.P., Adhikari, R., Barrow, C.J., Adhikari, B.2017. Digestion behaviour of chia seed oil encapsulated in chia seed protein-gum complex coacervates. Food Hydrocoll., 66, 71-81.

Toro-Sierra, J., Schumann, J., Kulozik, U.2013. Impact of spray-drying conditions on the particle size of microencapsulated whey protein fractions. Dairy Sci. Technol., 93, 487-503.

Treybal, R.E. 1980. Mass transfer operations, (3rd ed.), McGraw-Hill Book Company, Singapore.

Us-Medina, U., Julio, L.M., Segura-Campos, M.R., Ixtaina, V.Y., Tomás, M.C.2018. Development and characterization of spray-dried chia oil microcapsules using by-products from chia as wall material. Powder Technol., 334, 1–8.

Walton, D. E., Mumford, C.J.1999. The morphology of spray- dried particles – The effect of process variables upon the morphology of spray- dried particles. Chem. Eng. Res. Des., 77(A5), 442–460.

Walzel, P. 2012. Spraying and atomizing of liquids, Wiley-VCH (Ed.) Ullmann's Encyclopedia of Industrial Chemistry, Wiley-VCH Verlag GmbH &C,Weinheim, pp. 79–98.

Figure captions.

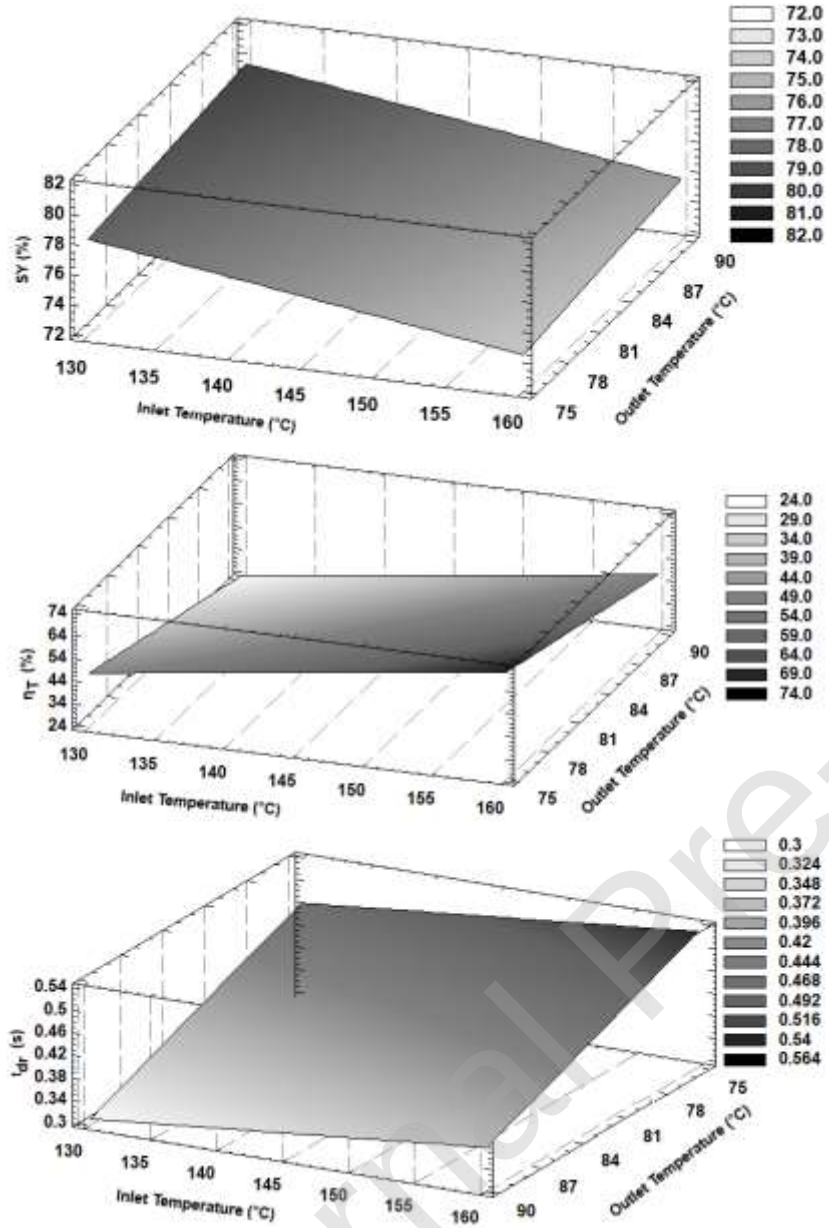

Figure 1. Estimated response surfaces for the solid yield (*SY*), thermal efficiency (η_T) and droplet evaporation time (t_{dr}).

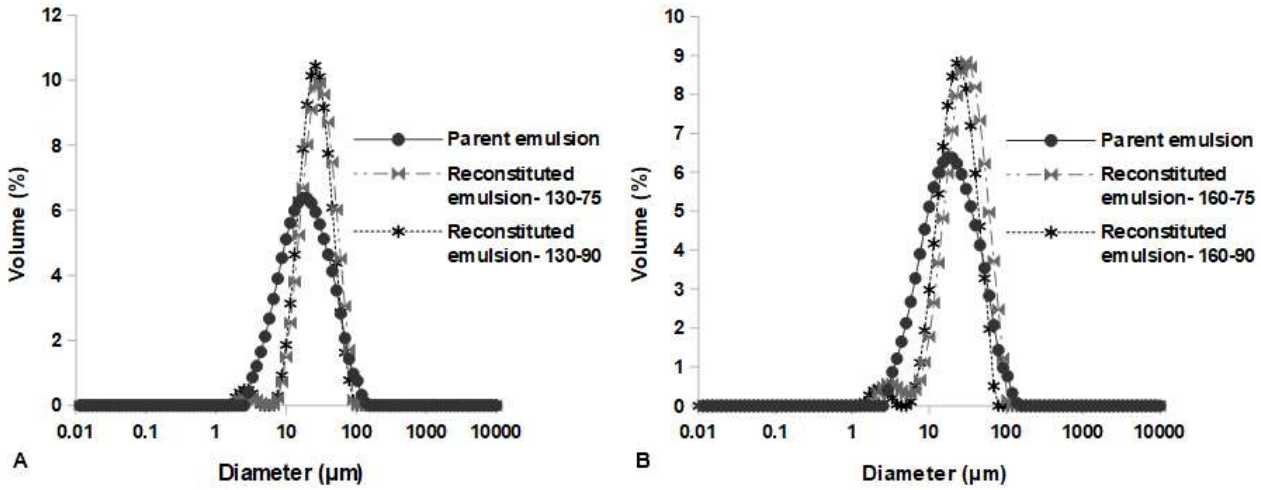

Figure 2. Oil droplet size distribution in parent and reconstituted emulsions. For a T_{inlet} of **A.** 130 °C and **B.** 160 °C. Drying conditions are indicated by a combination of T_{inlet}-T_{outlet}.

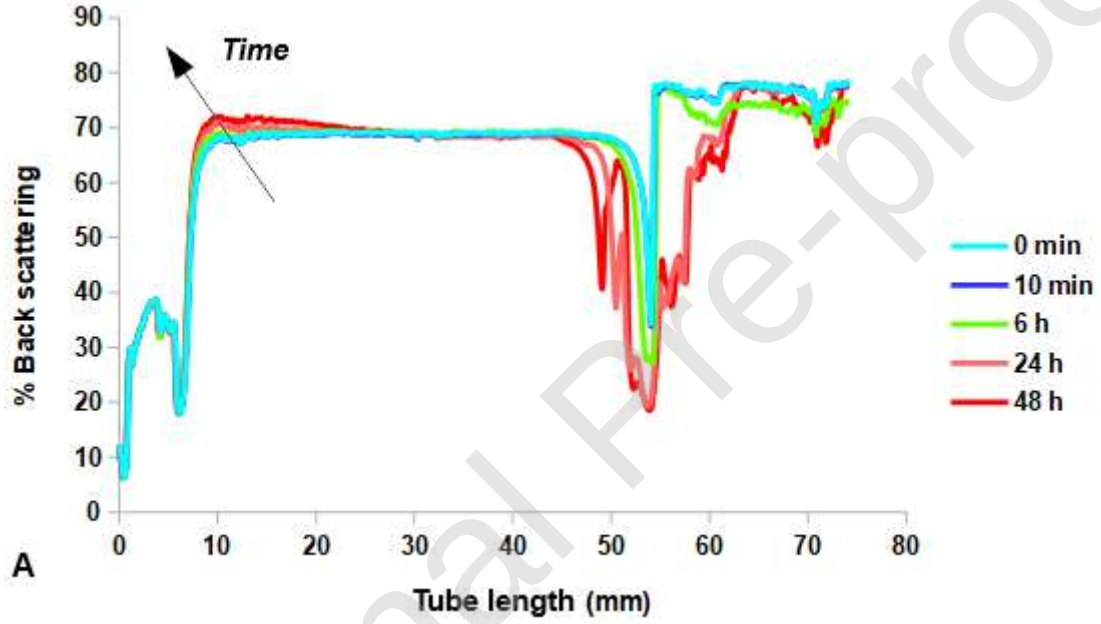

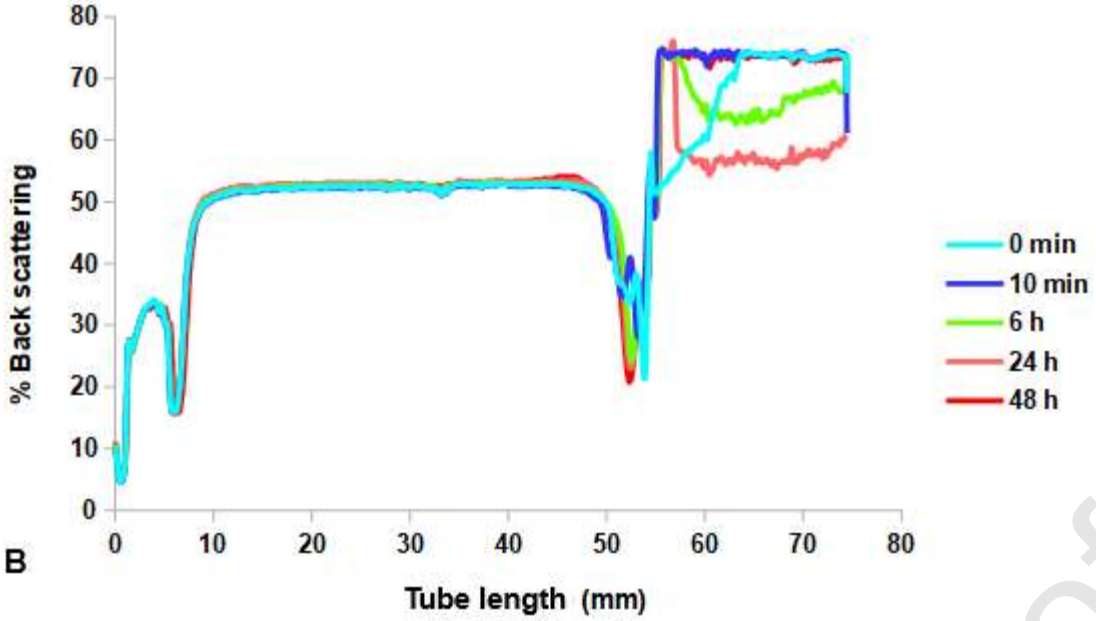

B

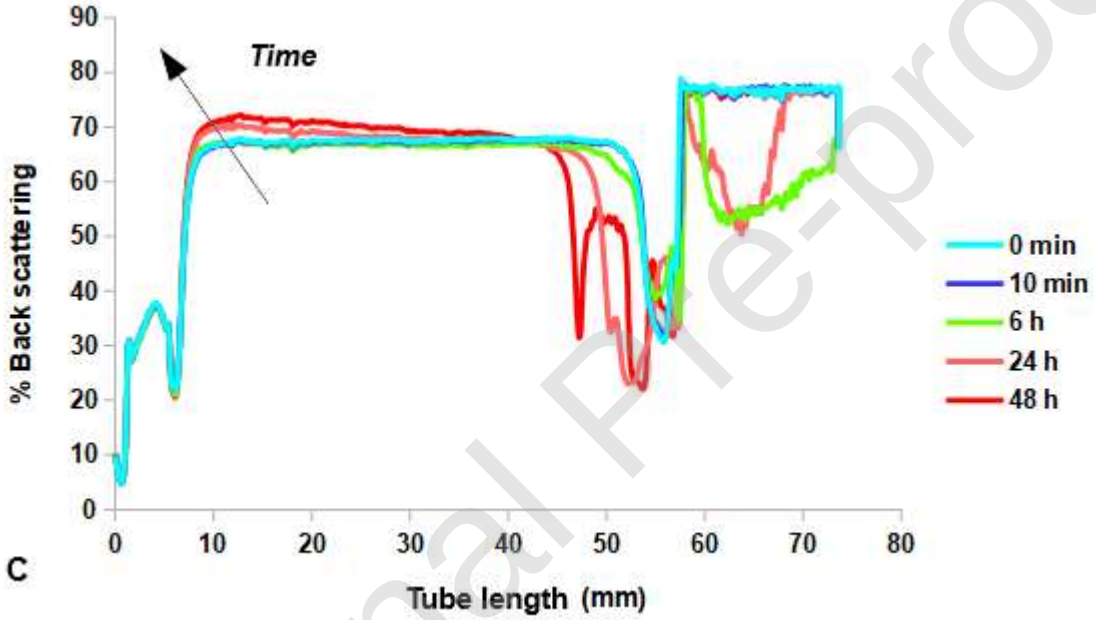

C

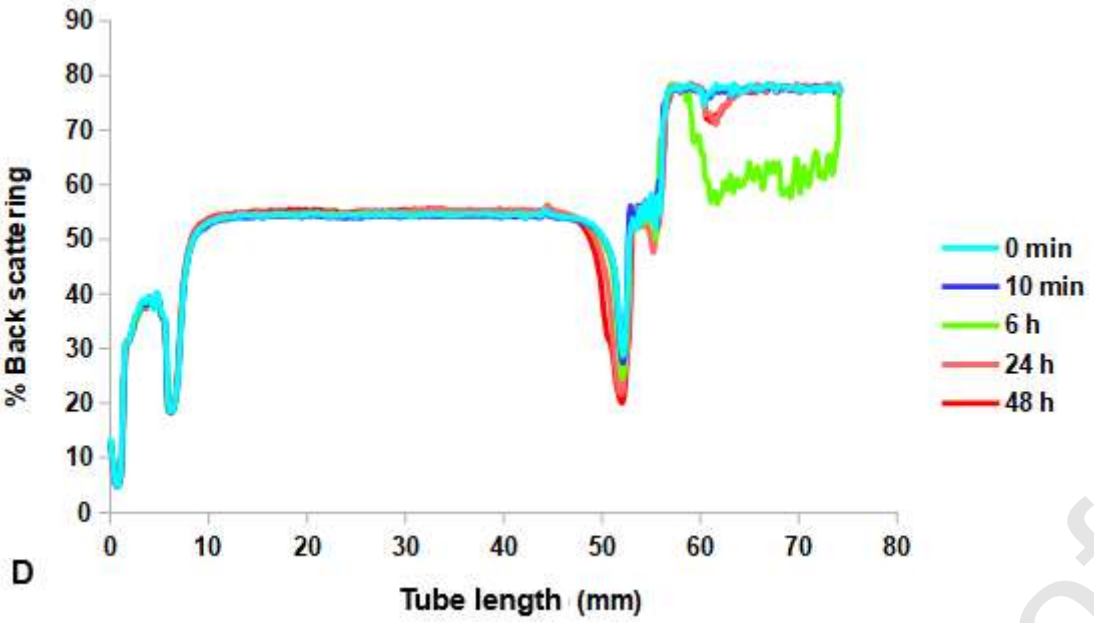

D

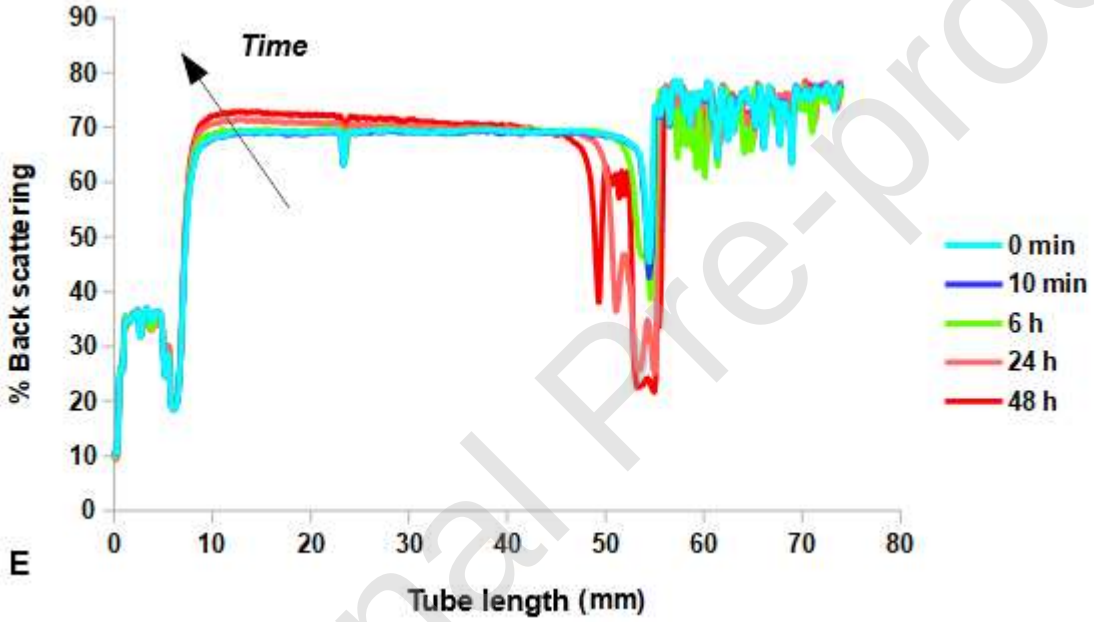

E

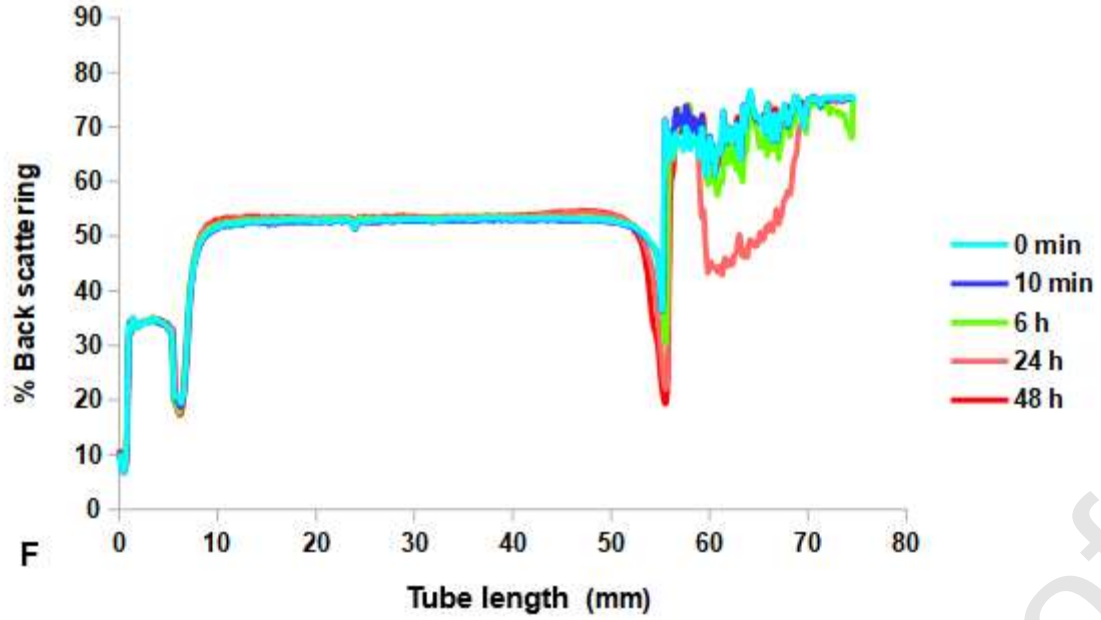

F

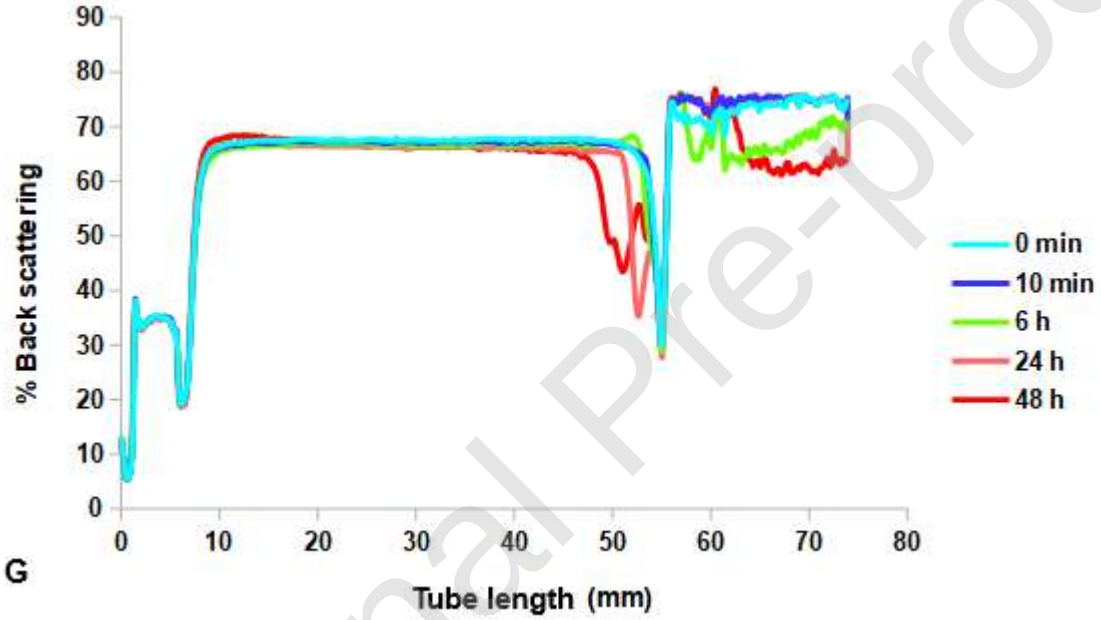

G

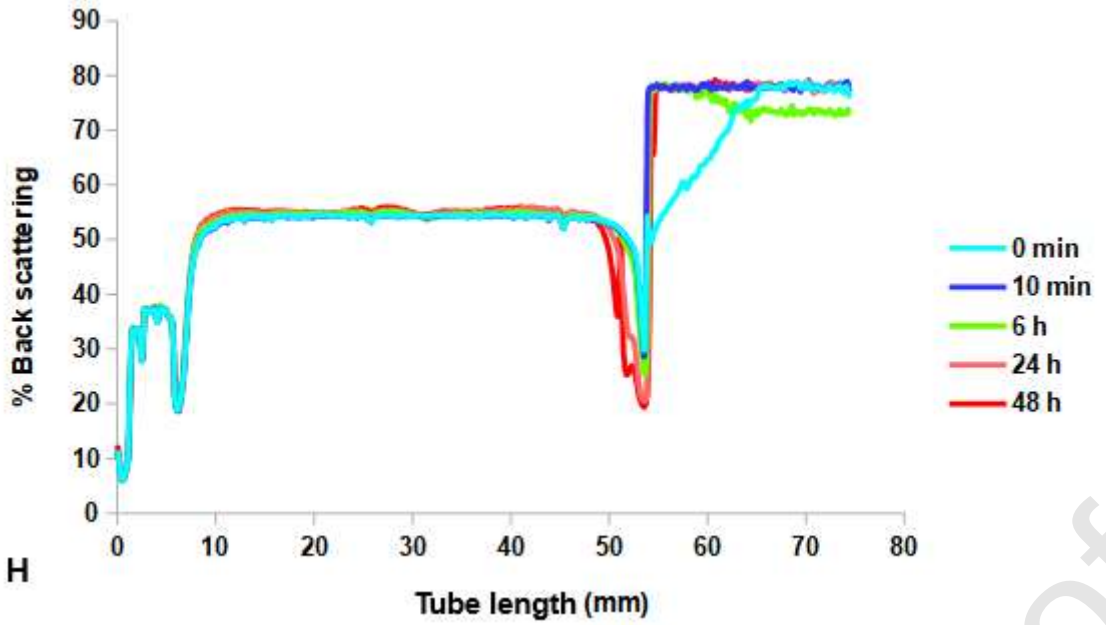

Figure 3. Back scattering profiles for reconstituted powders. Microcapsules: **A** (130-75 °C), **C** (130-90 °C), **E** (160-75 °C) and **G** (160-90 °C). Blank microparticles: **B** (130-75 °C), **D** (130-90 °C),**F**(160-75 °C) and **H** (160-90 °C).

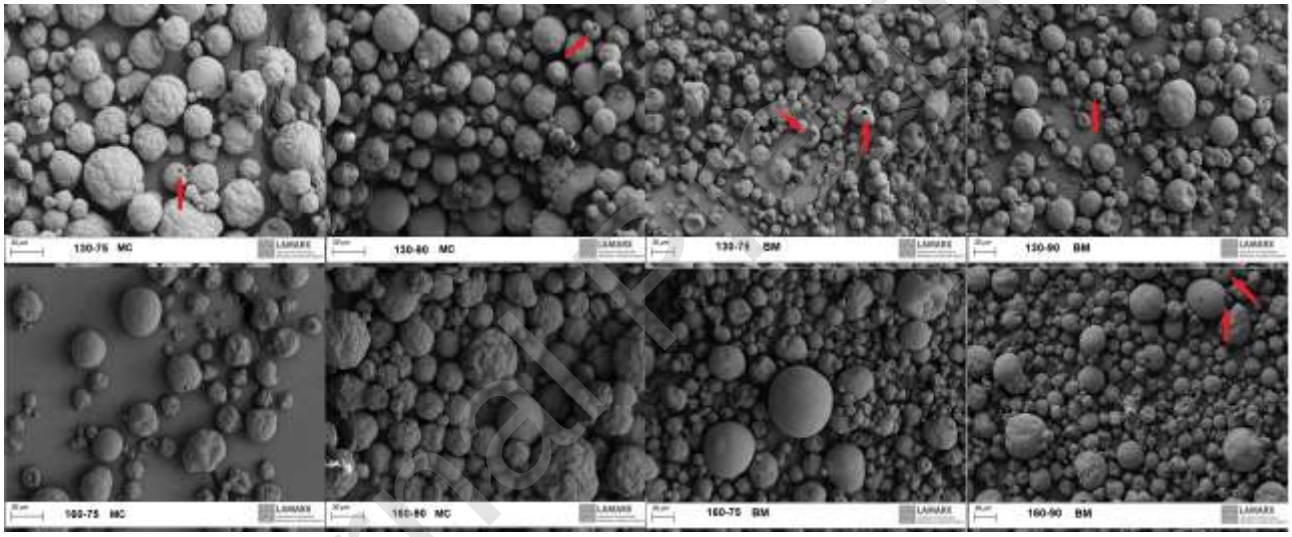

Figure 4. SEM images (380 x) of microcapsules (MC) and blank microparticles (BM). Drying conditions are indicated by a combination of T_{inlet}-T_{outlet}.

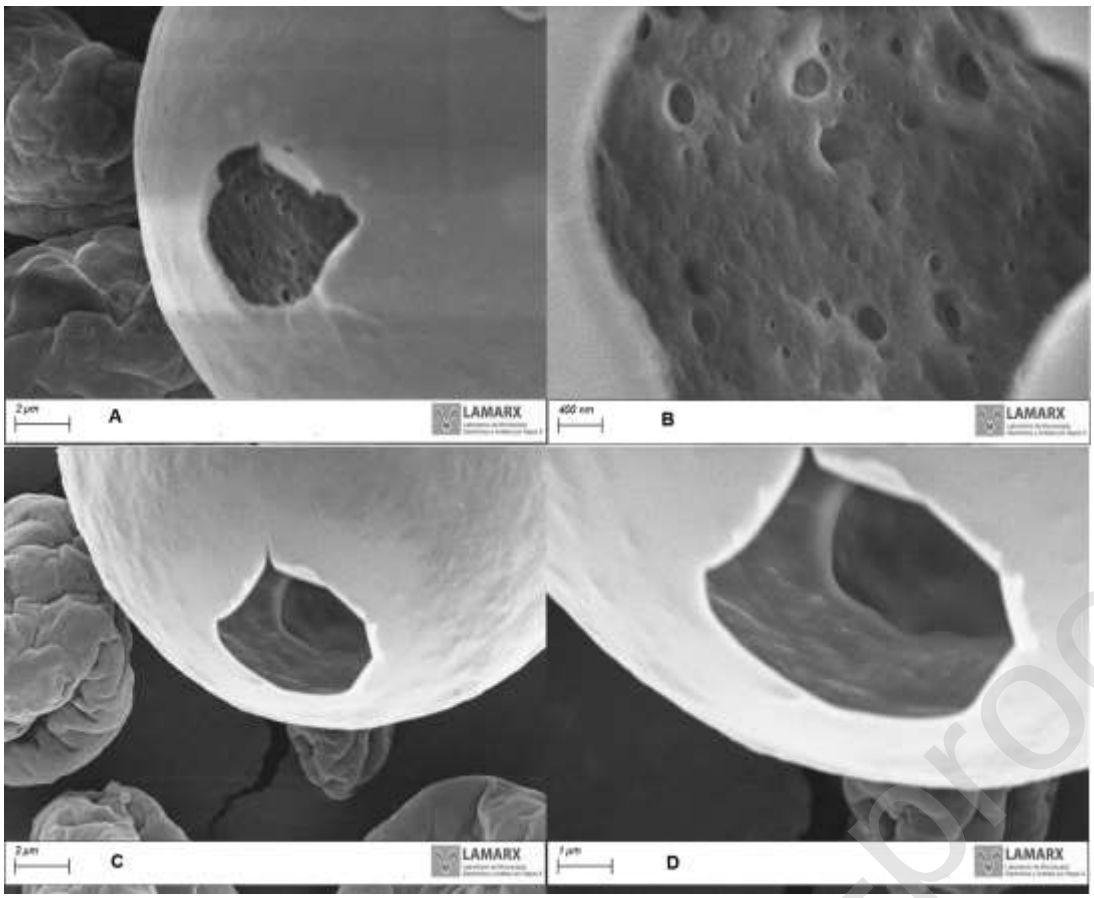

Figure 5. Internal microstructure of powders obtained at pilot-scale. Microcapsules (**A**, 5000 x and **B**, 11000 x) and blank microparticles (**C**, 5000 x and **D**, 11000 x).

Table 1. Composition of blank dispersions and O/W emulsions, and spray drying operating conditions.

	Blank dispersion	Emulsion
Composition, 100 mL		
CO		6 g
SPI	6 g	6 g
AG	6 g	6 g
MD	4 g	4 g
SPI/AG ratio w/w	1/1	1/1
[(SPI+AG)/CO] ratio w/w		2/1
Total solid content %w/v	16	22 (including CO)
Spray drying conditions		
Drying air inlet temperature, °C	130, 160	
Drying air outlet temperature, °C	75, 90	
Evaluated conditions, T_{inlet} x T_{outlet}	130 x 75 130 x 90 160 x 75 160 x 90	
Drying air mass flow rate, kg/h	390 (T_{inlet} =130 °C), 375 (T_{inlet} =160 °C)	
Atomizer wheel speed, rpm	25000	
Feed inlet temperature, °C	25	

CO, chia oil; SPI, soy protein isolate; AG, arabic gum; MD, maltodextrin.

Table 2. Results for the feed rate and the non dimensional flow rate per liquid thread.

	V_{feed}	V_{th}*
Process condition		
130-75	129.26^{b}±6.95	4.82^{b}±0.26
130-90	64.62^{a}±7.20	2.41^{a}±0.20
160-75	196.09^{c}±2.01	7.31^{c}±0.01
160-90	126.81^{b}±6.74	4.73^{b}±0.25

Each process condition is a combination of $T_{inlet\_}$ T_{outlet}, T_{inlet}, drying air inlet temperature (°C); T_{outlet}, drying air outlet temperature (°C); V_{feed}, volumetric feed rate (mL/min); V_{th}*, non dimensional flow rate per liquid thread (-). Different letters in each column indicate statistically significant ($p \leq 0.05$) differences among process conditions. Average (n=3) ± standard deviation are shown.

Table 3. Spray drying experimental design. Regression coefficients and results for the solid yield, thermal efficiency, droplet evaporation time and additional exposure time of dry particles.

	SY	η_T	t_{dr}	t_{cr}	t_{fr}	t_{EXP}
Regression Coefficient						
β_0	78.81	51.74**	1.00***	0.80***	0.19**	10.00***
β_1	-0.07*	0.79***	0.01*	0.01*	0.01**	-0.01*
β_2	0.21	-1.45***	-0.01***	-0.01***	-0.01***	0.01***
β_{12}						
R^2	0.94	0.97	0.94	0.94	0.93	0.94
SEE	0.99	4.24	0.03	0.02	0.00	0.03
MAE	0.51	2.99	0.02	0.01	0.01	0.02
Process condition						
130-75	78.07^{ab}±0.56	43.33^{b}±0.71	0.46^{a}±0.04	0.36^{a}±0.03	0.10^{b}±0.01	10.54^{a}±0.05
130-90	79.79^{b}±1.43	27.56^{a}±0.43	0.31^{b}±0.02	0.24^{b}±0.02	0.07^{a}±0.00	10.69^{b}±0.03
160-75	74.24^{a}±2.73	73.19^{d}±0.50	0.54^{a}±0.01	0.41^{a}±0.00	0.13^{cp}±0.00	10.46^{a}±0.01
160-90	75.63^{ab}±0.70	45.43^{c}±0.00	0.36^{b}±0.01	0.28^{b}±0.01	0.08^{ab}±0.00	10.63^{b}±0.01

Each process condition is a combination of $T_{inlet\_}$ T_{outlet}, T_{inlet}, drying air inlet temperature (°C); T_{outlet}, drying air outlet temperature (°C); β_0 is the constant term of the regression model; β_1 and β_2 are the linear coefficients corresponding to T_{inlet} and T_{outlet}, respectively; β_{12} is the interaction coefficient; R^2, determination coefficient; SEE, standard error of estimates; MAE, mean absolute error; *SY*, solid yield (%, dry basis); η_T, thermal efficiency (%); t_{dr}, droplet evaporation time (s); t_{cr}, droplet evaporation time corresponding to the constant rate period (s); t_{fr}, droplet evaporation time corresponding to the falling rate period (s); t_{exp}, additional exposure time of dry particles (s). Level of significance of the regression coefficients: *$p \leq 0.05$; **$p \leq 0.01$; ***$p \leq 0.001$. Different letters in each column indicate statistically significant ($p \leq 0.05$) differences among process conditions. Average (n=3) ± standard deviation are shown.

Table 4. Drying kinetic model. Estimated D[3,2], $D_{95,1}$ and critical diameters, and experimental $D_{95,2}$ (surface-weighted distribution) of dry microcapsules observed for each drying condition.

Process condition	D[3,2]	$D_{95,1}$	D_c	$D_{95,2}$
130-75	43.56±0.14	60.98±0.19	37.69±0.49	41.29±0.16
130-90	37.46±1.14	52.44±1.60	31.77±0.98	33.97±0.03
160-75	48.93±0.20	68.50±0.20	41.57±0.05	43.23±1.33
160-90	44.57±0.15	62.40±0.21	37.40±0.48	38.96±0.09

Each process condition is a combination of T_{inlet}–T_{outlet}, T_{inlet}, drying air inlet temperature (°C); T_{outlet}, drying air outlet temperature (°C);*D [3,2]* estimated Sauter mean diameter (µm) of the spray; $D_{95,1}$ estimated diameter corresponding to the 95th percentile of the size distribution in the spray (µm); D_C, estimated critical diameter (µm); $D_{95,2}$ observed diameter corresponding to the 95th percentile of the size distribution in dry microcapsules (µm). Average (n=3) ± standard deviation are shown.

Table 5. Spray drying experimental design. Regression coefficients and results for the physico-chemical properties of microcapsules.

		a_W	*MC*	*D [4,3]*	d_{50}*	*WI*	*CI*	*HR*	*EE*	*AO*	*IT*
Regression coefficient	β_0	-0.56	25.88	-9.79**	-2.69	274.31	-238.07	-2.33	85.70	1135.07	54.16
	β_1	0.01***	-0.13	0.41	0.04	-1.53	1.52*	0.02*	0.07	-7.06	-0.32*
	β_2	0.01	-0.27**	0.47**	0.05*	-2.71	3.29*	0.04*	0.07	-12.69*	-0.64
	β_{12}	-0.01***	0.01*	-0.01*	-0.01	0.02**	-0.02*	-0.01*	-0.01	0.08***	0.01*
R^2		0.99	0.97	0.98	0.91	0.98	0.94	0.95	0.96	0.99	0.95
SEE		0.00	0.12	0.51	0.07	0.52	1.65	0.02	1.15	1.23	0.26
MAE		0.00	0.06	0.26	0.03	0.29	0.99	0.01	0.60	0.70	0.13
Process condition											
130-75		0.30^{c}± 0.00	3.54^{c}± 0.08	28.28^{a}± 2.20	1.63^{ab}± 0.13	52.83^{b}± 0.49	9.54^{a}± 0.64	1.10^{a}± 0.00	96.97^{a}± 1.54	100^{d}± 0.00	5.59^{b}± 0.03
130-90		0.32^{d}± 0.00	2.44^{a}± 0.06	25.31^{a}± 1.92	1.54^{ab}± 0.00	48.45^{a}± 0.59	19.62^{b}± 1.02	1.24^{b}± 0.03	97.41^{a}± 0.87	76.58^{a}± 2.40	4.25^{a}± 0.06
160-75		0.27^{b}± 0.00	3.06^{b}± 0.04	28.87^{a}± 2.56	1.66^{b}± 0.14	48.63^{a}± 0.09	9.81^{a}± 0.27	1.11^{a}± 0.00	98.28^{a}± 0.91	80.75^{b}± 0.26	5.54^{b}± 0.03
160-90		0.25^{a}± 0.00	2.64^{ab}± 0.09	23.57^{a}± 1.36	1.35^{a}± 0.08	52.62^{b}± 0.49	10.83^{a}± 0.68	1.12^{a}± 0.00	98.57^{a}± 1.02	95.86^{c}± 1.30	6.11^{b}± 0.12

Each process condition is a combination of T_{inlet} – T_{outlet}, T_{inlet}, drying air inlet temperature (°C); T_{outlet}, drying air outlet temperature (°C); β_0 is the constant term of the regression model; β_1 and β_2 are the linear coefficients corresponding to T_{inlet} and T_{outlet}, respectively; β_{12} is the interaction coefficient; R^2, determination coefficient; SEE, standard error of estimates; MAE, mean absolute error; a_w water activity at 25 °C*; MC* moisture content (%, wet basis); *D [4,3]* de Brouckere mean diameter (µm); d_{50}* normalized value of the median diameter; *WI whiteness index*; *CI*, Carr Index; *HR* Hausner ratio; *EE* encapsulation efficiency (%, dry basis); *AO* available oil after *in vitro* digestion (%); *IT* induction time (h). Level of significance of the regression coefficients: *p ≤ 0.05; **p ≤ 0.01; ***p ≤ 0.001.
Different letters in each column indicate statistically significant (p≤0.05) differences among process conditions.
Average (n=3) ± standard deviation are shown.

Table 6. Multiple response optimization for the microencapsulation of chia oil. Goals, predicted and observed optimum values, and goodness-of-fit for the response variables.

	SY	η_T	t_{EXP}			
Goal	*Max*	*Max*	*Min*			
Predicted optimum	75.63	48.43	10.63			
Observed optimum	76.65±1.45	45.88±3.60				
AAD	0.01	0.07				
B_f	1.00	0.99				
A_f	1.01	1.07				

	a_W	*MC*	*D [4,3]*	d_{50}*	*WI*	*CI*
Goal	*Min*	*Min*	*Min*	*Min*	*Max*	*Min*
Predicted optimum	0.25	2.64	23.57	1.35	52.62	10.83
Observed optimum	0.25± 0.00	2.59±0.12	24.05±0.68	1.33±0.03	53.88±0.08	11.77±0.34
AAD	0.00	0.03	0.05	0.04	0.05	0.08
B_f	1.00	1.00	1.00	1.00	0.95	1.00
A_f	1.00	1.03	1.05	1.04	1.05	1.08

	HR	*EE*	*AO*	*IT*
Goal	*Min*	*Max*	*Max*	*Max*
Predicted optimum	1.12	98.57	95.86	6.11
Observed optimum	1.11±0.01	97.19±1.86	94.97±3.58	5.94±0.12
AAD	0.01	0.01	0.01	0.03
B_f	1.00	1.00	1.00	1.00
A_f	1.01	1.01	1.01	1.03

SY, solid yield (%, dry basis); η_T, thermal efficiency (%); t_{exp}, additional exposure time of dry particles (s); a_w water activity at 25 °C*; MC* moisture content (%, wet basis); *D [4,3]* de Brouckere mean diameter (μm); d_{50}* normalized value of the median diameter; *WI whiteness index*; *CI*, Carr Index; *HR* Hausner ratio; *EE* encapsulation efficiency (%, dry basis); *AO* available oil after *in vitro* digestion (%); *IT* induction time (h). *Min*, minimize; *Max*, maximize; *AAD*, absolute average deviation; B_f, bias factor; A_f, accuracy factor.

Table 7. Onset temperature (T_{onset}) and activation energy (E_a) for oxidation in bulk and microencapsulated chia oil.

Non-isotermic mode	***β***	***Bulk oil***	***MC-160-90***
T_{onset}	5	137.07[a]±1.13	165.97[b]±0.92
	10	157.44[a]±0.70	178.37[b]±2.01
	20	161.86[a]±0.25	188.70[b]±0.33
E_a		68.86[a]±2.09	97.00[b]±4.29
R^2		0.93	0.99

The drying condition is indicated by T_{inlet} –T_{outlet}, where, T_{inlet} is the drying-air inlet temperature (°C); T_{outlet} is the drying-air outlet temperature (°C); MC, microcapsule; β isthe heating rate (°C/min); T_{onset} is the onset temperature for primary oxidation (°C); E_a is the activation energy (kJ/mol); R^2 is a determination coefficient. Different letters in the same row indicate statistically significant differences ($p \leq 0.05$) between bulk and microencapsulated oils. Average (n=3) ± standard deviation are shown.

Table 8. Some properties of blank microparticles (without encapsulated chia oil).

	a_W	*MC*	*D [4,3]*	*WI*	*CI*	*HR*
Process condition						
130-75	0.31[b]± 0.00	5.30[c]± 0.15	18.41[a]± 0.37	53.18[ab]± 0.23	7.54[a]± 0.82	1.08[b]± 0.02
130-90	0.32[b]± 0.00	4.55[b]± 0.03	17.88[a]± 1.54	53.05[b]± 0.41	3.81[b]± 0.07	1.04[a]± 0.01
160-75	0.27[a]± 0.00	5.32[c]± 0.17	17.79[a]± 0.82	52.64[a]± 0.23	5.00[ab]± 0.00	1.05[ab]± 0.00
160-90	0.26[a]± 0.01	2.88[a]± 0.18	21.95[a]± 1.85	53.82[b]± 0.16	4.88[ab]± 0.17	1.05[ab]± 0.00

Each process condition is a combination of T_{inlet} – T_{outlet}, T_{inlet}, drying air inlet temperature (°C); T_{outlet}, drying air outlet temperature (°C); a_w water activity at 25 °C*; MC* moisture content (%, wet basis); *D [4,3]* de Brouckere mean diameter (μm); *WI whiteness index*; *CI*, Carr Index; *HR* Hausner ratio. Different letters in each column indicate statistically significant ($p \leq 0.05$) differences among process conditions. Average (n=3) ± standard deviation are shown.